

Pattern Formation in One and Two Dimensional Shape-Space Models of the Immune System

Rob J. De Boer[†], Lee A. Segel[‡] & Alan S. Perelson[†]

[†]Theoretical Division, Los Alamos National Laboratory
Mail Stop K710, Los Alamos, NM 87545, USA

[‡]Department of Applied Mathematics and Computer Science
The Weizmann Institute of Science, Rehovot 76100, Israel

Summary

We analyze a large-scale model of the immune network using the shape-space formalism. In this formalism, it is assumed that the immunoglobulin receptors on B cells can be characterized by their unique portions, or idiotypes, which have shapes that can be represented in a space of a small finite dimension. Two receptors are assumed to interact only when the shapes of their idiotypes are complementary. We model this by using a Euclidean metric and assuming that shapes interact whenever their coordinates in the space-space are of opposite sign. The range of the interaction is defined by a standard Gaussian function with variance σ^2 .

The degree of stimulation of a cell when confronted with complementary idiotypes is modeled using a log bell-shaped interaction function. This leads to three possible equilibrium states for each clone: a virgin, an immune, and a suppressed state. We study the stability properties of the three possible homogeneous steady states of the network. For the parameters chosen, the homogeneous virgin state is stable to both uniform and sinusoidal perturbations of small amplitude. A sufficiently large perturbation will however destabilize the virgin state and lead to an immune reaction. Thus, the virgin system is both stable and responsive to perturbations. The homogeneous immune state is unstable to both uniform and sinusoidal perturbations, whereas the homogeneous suppressed state is stable to uniform, but unstable to sinusoidal, perturbations. Using numerical methods we study the non-uniform patterns that arise from perturbations of the homogeneous states. Identifying with the *in vivo* situation, these patterns represent the actual immune repertoire of an animal. In contrast with most reaction-diffusion models, pattern formation in this model is not dependent on long-range inhibition and short-range activation.

Embedding our model in a one-dimensional shape-space, we numerically analyze the system upon varying the parameter σ . If σ is large compared to the size of the shape-space, the system attains a fixed non-uniform equilibrium. Conversely if σ is small, the system attains one out of many possible non-uniform equilibria, with the final pattern depending on the initial conditions. This demonstrates the plasticity of the immune repertoire in this shape-space model. We describe how the repertoire organizes itself into large clusters of clones having similar behavior.

We extend these results by analyzing pattern formation in a two-dimensional (2D) shape-space. To do this we use a lattice mapping whose rules are rigorously derived from a simplified version of the underlying differential equations via a logarithmic transformation of variables. A novel feature of the lattice model is that the neighborhood of cell (i, j) is centered around cell $(-i, -j)$. Thus interactions are nonlocal. The 2D patterns that we find are reminiscent of those found in reaction-diffusion systems with many hills and valleys. The scale of the pattern depends on neighborhood size, with small neighborhoods generating fine scale patterns with narrow peaks, and large neighborhoods generating large scale patterns with wide peaks and valleys. Both one and two-dimensional models support patterns in which a fraction of the clones are not stimulated by network interactions. The fraction of such "disconnected clones" increases with both dimensionality and σ .

Introduction

Jerne (1974) postulated that the immune system functions as a network with a complexity comparable to that of the nervous system. The number of different lymphocyte clones, or idiotypes, involved in the immune network may be of order 10^6 to 10^8 . Interactions amongst the clones depend on complementarities between the different immunoglobulin receptors characteristic of each clones. The degree of binding of two idiotypes, usually measured by their equilibrium binding constant or affinity, depends on the generalized shapes of the two receptor molecules involved (Perelson & Oster, 1979). By generalized shape, we mean not only the average geometric shape of the binding region of the receptor molecule, but also factors such as the electric charge, dipole moments, and hydrophobicity. Recent structural determinations of antigen-antibody complexes (cf., Amit *et al.*, 1986; Stanfield *et al.*, 1990) highlight the importance of shape complementarity and show that in the binding region positive charges are complemented by negative ones (Sheriff *et al.*, 1987). Because cells in the immune system are constantly being generated in the bone marrow, stimulated to grow, and dying, one is led to conceive of the immune network as a vast collection of shifting clonal populations each characterized by a generalized shape x .

Our attempts to model high-dimensional immune networks have utilized two different approaches to represent molecular shape and to compute complementarity between molecules. In one approach, we have associated the shape of receptors with a binary string, and used the degree of complementarity between bitstrings to determine the degree of interaction between clones. The degree of interaction is then used to generate terms in a system of ordinary differential equations that determines the population size of each clone. In this approach the number of idiotypes incorporated in the network can vary, owing to the introduction of novel clones from a source meant to mimic the bone marrow, and owing to interactions among the clones present in the network (Farmer *et al.*, 1986; De Boer & Perelson, 1991). In a second approach put forward by Segel & Perelson (1988), and which we shall pursue here, shape is described by a vector of real numbers and a set of partial differential equations in both shape and time variables determines the size of clonal populations. A typical rule to determine complementarity is that a receptor of shape x is complementary to a receptor of shape $-x$. By finite difference methods, the

partial differential equations can be converted into a set of ordinary differential equations. Thus, a discrete set of equations results but these are different from those in the bitstring model in that they have a different interaction kernel.

It is conceivable that an adequate characterization of essential shape variables can be accomplished by a relatively small number of measurements (Perelson & Oster, 1979). This gives a shape-space of some small finite dimension. Our earlier work (Segel & Perelson, 1988) was confined to a one-dimensional (1D) shape-space; here we will extend this to a two-dimensional (2D) shape-space. By contrast, in the bitstring approach the shape-space is the ℓ -dimensional hypercube, where ℓ is the number of bits in the string used to represent shape. As we demonstrate below the advantage of using a continuous shape-space is that standard analytical methods are available for analyzing system behavior.

The model that we analyze here is the simplest of a sequence of models that we have proposed, and studied extensively, in previous publications (De Boer 1988; De Boer & Hogeweg, 1989a-c; De Boer *et al.*, 1990; De Boer & Perelson, 1991; Perelson and Weisbuch, 1991; Weisbuch *et al.*, 1990). For each B cell population, the model incorporates one differential equation with terms corresponding to (1) a constant source of cells from the bone marrow, (2) cell death, and (3) proliferation in response to cell activation. The most crucial feature of the model is that the degree of activation is a log bell-shaped function of the total amount of stimulation a cell receives. Since a bell-shaped function has a region in which it increases and a region in which it decreases, the effect of increasing the stimulation can either be an increase or a decrease in proliferation. A steady state exists in each of the two regions. We have called these the *immune state* and the *suppressed state*, respectively. A third steady state exists when the degree of stimulation is low. This *virgin state*, is characterized by a balance between the source of cells from the bone marrow and the loss of cells due to cell death.

Here we study this model in a shape-space setting. Our aim is to come to a better understanding of repertoire development. The potential repertoire of our model immune system is the entire shape-space. Owing to network interactions, some regions of the shape-space will be suppressed, some will be activated, and some will hardly be stimulated by other shapes in the immune network. Accordingly, we expect some spatial distribution of clone sizes throughout the network, where "spatial" refers to shape-space. This distribution, together with the spatial distribution of the degree of stimulation, defines our immune repertoire. We will show that the repertoire is very plastic in the sense that it can assume any of a large number of distinct spatial distributions. Further, we analyze the onset of pattern formation via linear stability theory. We find that the formation of patterns in the immune repertoire does not require different ranges of inhibition and activation.

The most important immunological question that we address is whether or not the network, in its shape-space setting, will be able to combine a functional idiotypic network with a clonal organization of functionally disconnected antigen-reactive clones. In two recent reviews, Coutinho (1989) and Holmberg *et al.* (1989) argue that about 10-20% of

clones form an idiotypic network. In their view, the other 80–90% of clones are disconnected from the network and form a clonal compartment of immunocompetent but resting lymphocytes that is responsible for immune responses to foreign antigens. The network is thought to select which T and B cell clones are expressed in an animal. This is what we call *repertoire selection*. In a shape-space model, the question of finding a combination of network and independent clonal organizations boils down to finding a mosaic of regions that are stimulated by the network and regions that are hardly stimulated. We will show this to be possible, but in our model the fraction of cells in each compartment does not agree with the Coutinho-Holmberg estimates.

The outline of this paper is as follows. We will first introduce the 1D shape-space version of our model, and discuss its three uniform equilibrium states. We analyze the stability properties of these three states to both uniform and sinusoidal perturbations of small amplitude. We numerically study the model and then, based on our results, modify the model by introducing density dependent growth to give more realistic non-uniform patterns. We then analyze a two-dimensional version of the model using a 2D lattice mapping. Readers unfamiliar with mathematical analysis may wish to skip the sections dealing with the stability of the uniform steady states.

Model

Our model is composed of an infinite number of B cell populations of different shapes that may be ordered in a finite-dimensional shape-space. In order to facilitate analytic treatment we study a simple version of our idiotypic network model, in which we do not differentiate between B cells and free antibody, and in which we use a phenomenological log bell-shaped function to summarize the chemistry involved in receptor crosslinking and subsequent B cell activation. We have previously shown that more complex models that incorporate antibodies and crosslinking chemistry have similar steady states but in some parameter regimes tend to have oscillatory and/or chaotic behavior (De Boer *et al.*, 1990; Perelson & Weisbuch, 1991). Free antibody can be imagined as present, if one assumes that there is always a constant number of free antibodies per lymphocyte. Note, however, that we have shown before that this can be an unrealistic assumption (De Boer & Perelson, 1991). An analysis with this assumption lifted will be published elsewhere (Perelson & Segel, 1991).

In our model we consider B cell populations, $b(x, t)$, with receptors of shape x at time t . Although x may be a vector in R^n , we mainly consider only the simplest case wherein x is a real number bounded by the half-length, L , of shape-space, i.e., $-L \leq x \leq L$. In the analysis that follows we will indicate places in which the treatment would need to be varied for higher dimensional shape-spaces. Weisbuch (1990) and Weinand (1990, 1991) have explicitly dealt with two and three dimensional shape-spaces; Percus (1988) presents a model in which the dimension need not be specified. High dimensional models restricted to a Bethe lattice have also been presented by Percus (1989) and Weisbuch *et al.* (1990).

Recently Stewart and Varela (submitted) present a 2D shape-space model resembling the one presented here. Their model is further addressed in the Discussion.

Writing $b(x, t)$ as b , we propose as the fundamental population balance equation of our model

$$\frac{\partial b}{\partial T} = M + b(Pf(h) - d).$$

Here M is the constant source of cells from the bone marrow, d is the per capita rate of cell death, P is the maximum per capita rate of B cell proliferation, $f(h)$ defines the degree of activation, and h is the total stimulation that the population receives from all other B cell populations in the shape-space. We will refer to h as the *external field* or simply the *field* of the population. The model is non-dimensionalized by scaling the time T to the rate at which B cells turn over,

$$\frac{\partial b}{\partial t} = m + b(pf(h) - 1), \quad (1)$$

where $t = Td$, $m = M/d$, and $p = P/d$.

The most crucial feature of this model is the shape of the activation function $f(h)$, which is taken to be a biphasic dose-response function (Fig. 1)

$$f(h) = \frac{h}{\theta_1 + h} \left(1 - \frac{h}{\theta_2 + h}\right) = \frac{h}{\theta_1 + h} \frac{\theta_2}{\theta_2 + h}, \quad (2)$$

where $\theta_2 \gg \theta_1$. The first factor in h increases from 0 to 1, reaching its half-maximal value at θ_1 , the second factor decreases from 1 to 0, reaching its half-maximal value at θ_2 . For $\theta_2 \gg \theta_1$, the maximum $\frac{\theta_2}{(\sqrt{\theta_1} + \sqrt{\theta_2})^2}$, is approximately one. This maximum is attained at $h = \sqrt{\theta_1 \theta_2}$. Because $0 \leq f(h) < 1$, we derive from Eq. (1) that the B cells can maximally grow at a rate $p - 1$. Thus, in order to allow for net clonal expansion p must be greater than 1. Since maximally stimulated cells divide about once every 16 h, and cells live a few days (e.g. $d = 0.5 \text{ d}^{-1}$), $p = 2$ is a typical non-dimensional rate of proliferation.

Below the maximum of $f(h)$, increasing h increases $f(h)$; we call this the *stimulatory regime*. Above the maximum, increasing h decreases $f(h)$; we call this the *suppressive regime*. Plotted as a function of $\log h$, the graph of $f(h)$ is a bell-shaped curve (Fig. 1). An important argument for the use of a log bell-shaped function is that receptor crosslinking is involved in B cell activation. The fraction of cell surface receptors cross-linked by a ligand when plotted against the logarithm of the ligand concentration is called a cross-linking curve. For bivalent ligands the cross-linking curve is bell-shaped and symmetric around its maximum (Dembo & Goldstein, 1978; Perelson & DeLisi, 1980; Perelson, 1984).

The field $h(x, b)$ that is felt by B cells of shape x determines the degree of cell stimulation. To specify the field, we assume cells of shape x are stimulated by cells of complementary shape centered around $\hat{x} = -x$. For any shape x , let $g(x, \hat{x})b(\hat{x}, t)d\hat{x}$ be the total

stimulation (or field), h , that B cells of shape x receive from B cells of shapes between \hat{x} and $\hat{x} + d\hat{x}$, where $d\hat{x}$ is a small number. Then

$$h(x, b) = \int_{-L}^L g(x, \hat{x}) b(\hat{x}, t) d\hat{x} . \quad (3)$$

As in Segel & Perelson (1988), we assume that affinity or degree of interaction between shapes x and \hat{x} decreases according to a Gaussian function $g(x, \hat{x})$ of the distance to the perfect match $x = -\hat{x}$:

$$g(x, \hat{x}) = G(2\pi\sigma^2)^{-1/2} \exp[-(x + \hat{x})^2/2\sigma^2] , \quad (4)$$

where G and σ are constants determining the amplitude and width of the function, respectively. If each shape is complementary to only a small fraction of all possible shapes, $\sigma \ll L$. Because we can scale θ_1 , and θ_2 , we can set $G = 1$ without loss of generality (De Boer & Perelson, 1991). This has the advantage that for $L \gg \sigma$

$$\int_{-L}^L g(x, \hat{x}) d\hat{x} \approx 1 . \quad (5)$$

For a multidimensional shape-space, we replace Eq. (4) with

$$g(\mathbf{x}, \hat{\mathbf{x}}) = G(2\pi\sigma^2)^{-\ell/2} \exp[-(\mathbf{x} + \hat{\mathbf{x}})^2/2\sigma^2] ,$$

where ℓ is the dimension of the shape-space and \mathbf{x} and $\hat{\mathbf{x}}$ are ℓ -dimensional vectors. Using different variances in different shape-space directions is also possible in this multidimensional model.

Equilibrium states. We have shown before (De Boer, 1988; Weisbuch *et al.*, 1990) that whenever $m \ll \theta_1 \ll \theta_2$ Eq. (1) has three spatially uniform equilibria. We have called these the *virgin*, the *immune*, and the *suppressed* state respectively. In the shape-space each equilibrium corresponds to a uniform state in which all B cell populations are equal, i.e., $b(x) = \bar{b}$. By Eqs. (3) and (5) this means that the fields, $h(x, \bar{b}) = \bar{b} = \text{constant}$, for all x . Each of the three states has its own typical range of values of the field. We greatly simplify our analysis by approximating $f(h)$ differently in each of the three states.

The virgin state corresponds to a situation in which B cells are hardly stimulated. This corresponds to the first region of the bell-shaped function where $h \ll \theta_1 \ll \theta_2$ and

$$f(h) \approx \frac{h}{\theta_1} . \quad (2a)$$

Recalling that for a uniform state, $h = \bar{b}$, the equilibrium value, \bar{b} , of the virgin state is then given by

$$\frac{\partial \bar{b}}{\partial t} = 0 = m + \frac{p}{\theta_1} \bar{b}^2 - \bar{b} ,$$

with solutions

$$\bar{b}^{\pm} = \frac{1 \pm \sqrt{1 - 4mp/\theta_1}}{2p/\theta_1} . \quad (6)$$

Thus, the condition for having a virgin state is that $\sqrt{1 - 4mp/\theta_1}$ is real, or

$$4mp < \theta_1. \quad (7)$$

Whenever Eq. (7) holds, Eq. (6) has two real positive solutions. The virgin state corresponds to the smaller of the two, i.e., to \bar{b}^- . (The solution \bar{b}^+ is close to θ_1 and thus violates the condition $h \ll \theta_1$.) Choosing $m \ll \theta_1$, we approximate $\sqrt{1 - 4mp/\theta_1}$ by its first order Taylor expansion, and obtain

$$\bar{b}^- \approx m. \quad (8)$$

Since we choose $m \ll \theta_1$, Eq. (2a) is a good approximation of Eq. (2).

In the immune and the suppressed states B cells proliferate. Since a proliferating population based upon Eq. (1) expands mainly by cell division, and not by receiving novel cells from the bone marrow, we neglect m and observe that to a good approximation

$$\bar{b}(p(f(h) - 1) = 0, \quad \text{or} \quad f(h) = \frac{1}{p}, \quad \text{for} \quad \bar{b} > 0. \quad (9)$$

The immune state corresponds to a situation in which further stimulation, i.e., a small increase of h , increases the rate of proliferation. This corresponds to the increasing region of $f(h)$ where $h < \sqrt{\theta_1\theta_2}$. If $\sqrt{\theta_1\theta_2} \ll \theta_2$, i.e., if $\sqrt{\theta_1} \ll \sqrt{\theta_2}$, then $\theta_2/(\theta_2 + h) \approx 1$. Thus, we assume $\sqrt{\theta_1} \ll \sqrt{\theta_2}$, and in the region $m \ll h < \sqrt{\theta_1\theta_2} \ll \theta_2$, we approximate Eq. (2) by

$$f(h) = \frac{h}{\theta_1 + h}. \quad (2b)$$

Since $h = \bar{b}$, Eq. (9) becomes

$$f(h) = \frac{\bar{b}}{\theta_1 + \bar{b}} = \frac{1}{p},$$

and hence

$$\bar{b} = \frac{\theta_1}{p - 1}. \quad (10)$$

Note that because $p > 1$, $\bar{b} > 0$.

The suppressed state corresponds to situation in which further stimulation, i.e. an increase of h , decreases the rate of proliferation. This corresponds to the decreasing region of $f(h)$ where $h > \sqrt{\theta_1\theta_2}$. Therefore, by arguments similar to those given above, we approximate Eq. (2) by

$$f(\bar{b}) = \frac{\theta_2}{\theta_2 + \bar{b}}. \quad (2c)$$

Since $h = \bar{b}$, Eq. (9) becomes

$$f(h) = \frac{\theta_2}{\theta_2 + \bar{b}} = \frac{1}{p},$$

and hence

$$\bar{b} = (p - 1)\theta_2. \quad (11)$$

Because $p - 1 \approx 1$, the B cell population levels in the immune state, Eq. (10), and the suppressed state, Eq. (11), are located around the respective half-saturation constants, θ_1 and θ_2 , of the two saturation functions that make up $f(h)$.

The One-dimensional shape-space: Stability Analysis

The linear stability analysis that we perform below follows that given in Segel & Perelson (1988) for a similar model having only one uniform equilibrium state. Treating each of our three equilibria separately, we analyze stability to first uniform and then sinusoidal perturbations. This is necessary since, as we shall see, in this model in which the shape $x = 0$ is distinguished the system response to an infinite wavelength sinusoidal perturbation need not be the same as the response to a uniform perturbation. This has been noted before (Segel & Perelson, 1990).

Stability to uniform perturbations. We first examine the effect of a small perturbation $b'(t)$ that is applied to each B cell population. For each of the equilibria

$$0 = m + \bar{b}(pf(\bar{b}) - 1). \quad (12)$$

Writing

$$b(t) = \bar{b} + b'(t) \quad (13)$$

we find that

$$\frac{\partial(\bar{b} + b')}{\partial t} = \frac{\partial b'}{\partial t} = m + (\bar{b} + b')(pf(\bar{b} + b') - 1). \quad (14)$$

Upon substituting the first order Taylor expansion of $f(\bar{b} + b')$, employing Eq. (12), and neglecting the second order terms in b' we obtain

$$\frac{\partial b'}{\partial t} = b'(pf(\bar{b}) + \bar{b}pf'(\bar{b}) - 1),$$

where $f'(\bar{b})$ denotes the derivative of $f(h)$ with respect to h evaluated at $h = \bar{b}$. For stability we require $\partial b'/\partial t < 0$ when $b' > 0$, i.e.,

$$pf(\bar{b}) + \bar{b}pf'(\bar{b}) - 1 < 0. \quad (15)$$

For the virgin state, $\bar{b} = m$ Eq. (8), we approximate the log bell-shaped function Eq. (2) by its linear part, Eq. (2a), and obtain

$$f(m) = \frac{m}{\theta_1}, \quad f'(m) = \frac{1}{\theta_1}.$$

Thus, the stability condition Eq. (15) becomes

$$2pm < \theta_1. \quad (16a)$$

This stability condition is even less restrictive than condition Eq. (7) for having a virgin state. Since $p \approx 2$, and $m \ll \theta_1$ both conditions will be satisfied. We conclude that the virgin state is stable to uniform perturbations. The stability properties of the three steady states are summarized in Table 1.

For the immune state, $\bar{b} = \frac{\theta_1}{p-1}$ we approximate Eq. (2) by Eq. (2b), i.e., by the full stimulatory region of $f(h)$,

$$f(\bar{b}) = \frac{\bar{b}}{\theta_1 + \bar{b}} \quad , \quad f'(\bar{b}) = \frac{\theta_1}{(\theta_1 + \bar{b})^2} .$$

Thus, the stability condition Eq. (15) becomes

$$\frac{p-1}{p} < 0 . \quad (16b)$$

Since $p > 1$ the stability condition is never satisfied. We conclude that the immune state is unstable to uniform perturbations (see Table 1).

For the suppressed state, $\bar{b} = (p-1)\theta_2$, we approximate Eq. (2) by Eq. (2c), i.e., the decreasing region of $f(h)$,

$$f(\bar{b}) = \frac{\theta_2}{\theta_2 + \bar{b}} \quad , \quad f'(\bar{b}) = -\frac{\theta_2}{(\theta_2 + \bar{b})^2} .$$

Thus, the stability condition Eq. (15) becomes

$$-\left(\frac{p-1}{p}\right) < 0 . \quad (16c)$$

Since $p > 1$ the stability condition is always satisfied. We conclude that the suppressed state is stable to uniform perturbations (see Table 1).

Stability to sinusoidal perturbations. Now consider a perturbation that is exponential in time and sinusoidal in space. For that purpose consider a shape-space of infinite domain. We search for perturbations that can destabilize the uniform steady-states. We propose

$$b'(x, t) = e^{\lambda t} [\beta e^{ikx} + \beta^* e^{-ikx}] , \quad (17)$$

where the asterisk denotes the complex conjugate, and k is the wavenumber of the perturbation. In higher dimensions, we use a similar perturbation but replace kx by $\mathbf{k} \cdot \mathbf{x}$, where \mathbf{k} and \mathbf{x} are vectors. We assume $k \neq 0$, so that the perturbation is sinusoidal and leaves the average value of b unchanged. Employing Eqs. (3) and (17), and redefining the Gaussian function as $g(x + \hat{x})$, the perturbation of the field h due to b' is

$$\begin{aligned} h(b') &= e^{\lambda t} \int_{-\infty}^{\infty} g(x + \hat{x}) [\beta e^{ik\hat{x}} + \beta^* e^{-ik\hat{x}}] d\hat{x} \\ &= e^{\lambda t} \int_{-\infty}^{\infty} g(z) [\beta e^{ik(z-x)} + \beta^* e^{-ik(z-x)}] dz \\ &= e^{\lambda t} \hat{g}(k) [\beta e^{-ikx} + \beta^* e^{ikx}] . \end{aligned} \quad (18)$$

Here \hat{g} is the Fourier transform

$$\hat{g}(k) = \int_{-\infty}^{\infty} e^{ikz} g(z) dz = e^{-k^2 \sigma^2 / 2} . \quad (19)$$

In analogy to Eqs. (12-14) we write

$$\frac{\partial(\bar{b} + b')}{\partial t} = \frac{\partial b'}{\partial t} = m + (\bar{b} + b') \left[pf \left(\int g(x + \hat{x})(\bar{b} + b'(\hat{x})) d\hat{x} \right) - 1 \right].$$

Employing Eq. (5) we reshuffle this into

$$\frac{\partial b'}{\partial t} = m + (\bar{b} + b') \left[pf \left(\bar{b} + \int g(x + \hat{x}) b'(\hat{x}) d\hat{x} \right) - 1 \right],$$

which, upon expanding $f(\cdot)$ around \bar{b} yields

$$\frac{\partial b'}{\partial t} = m + (\bar{b} + b') \left[pf(\bar{b}) + pf'(\bar{b}) \int g(x + \hat{x}) b'(\hat{x}) d\hat{x} - 1 \right].$$

Neglecting the second order term of b' , and using Eq. (12), this can be rewritten as

$$\frac{\partial b'}{\partial t} = b' [pf(\bar{b}) - 1] + \bar{b} pf'(\bar{b}) \int g(x + \hat{x}) b'(\hat{x}) d\hat{x}.$$

Employing Eqs. (17) & (18) and cancelling $e^{\lambda t}$, this becomes

$$\lambda [\beta e^{ikx} + \beta^* e^{-ikx}] = [\beta e^{ikx} + \beta^* e^{-ikx}] (pf(\bar{b}) - 1) + [\beta e^{-ikx} + \beta^* e^{ikx}] \bar{b} pf'(\bar{b}) \hat{g}(k).$$

Thus,

$$0 = (pf(\bar{b}) - 1 - \lambda) [\beta e^{ikx} + \beta^* e^{-ikx}] + \bar{b} pf'(\bar{b}) \hat{g}(k) [\beta e^{-ikx} + \beta^* e^{ikx}].$$

For $k \neq 0$, the coefficient of $\exp(ikx)$ must vanish separately from the coefficient of $\exp(-ikx)$. Thus,

$$\beta (pf(\bar{b}) - 1 - \lambda) + \beta^* \bar{b} pf'(\bar{b}) \hat{g}(k) = 0, \quad (20a)$$

$$\beta^* (pf(\bar{b}) - 1 - \lambda) + \beta \bar{b} pf'(\bar{b}) \hat{g}(k) = 0. \quad (20b)$$

Subtracting the complex conjugate of Eq. (20b), $\beta (pf(\bar{b}) - 1 - \lambda^*) + \beta^* \bar{b} pf'(\bar{b}) \hat{g}(k)$, from Eq. (20a) yields

$$\beta (\lambda^* - \lambda) = 0.$$

For $\beta \neq 0$, this means that λ is real and that the behavior in time is monotonic. Since λ is real, Eqs. (20a & 20b) are merely each others complex conjugates. Splitting β into its real and imaginary parts

$$\beta \equiv \beta_r + i\beta_i,$$

and taking the real and imaginary parts of Eq. (20a) we obtain

$$\beta_r [pf(\bar{b}) - 1 - \lambda + \bar{b} pf'(\bar{b}) \hat{g}(k)] = 0,$$

$$\beta_i [pf(\bar{b}) - 1 - \lambda - \bar{b} pf'(\bar{b}) \hat{g}(k)] = 0.$$

Nontrivial solutions result when

$$\beta_r = 0, \beta_i \neq 0, \lambda = \lambda^- \quad \text{and} \quad \beta_r \neq 0, \beta_i = 0, \lambda = \lambda^+, \quad (21)$$

where

$$\lambda^\pm = pf(\bar{b}) - 1 \pm \bar{b} pf'(\bar{b}) e^{-k^2 \sigma^2 / 2}, \quad k \neq 0, \quad (22)$$

and Eq. (19) has been used to substitute for $\hat{g}(k)$. We now use this result, i.e., the values of λ^+ and λ^- , to examine the stability of the virgin, immune, and suppressed steady states to sinusoidal perturbations.

In the virgin state, $\bar{b} \approx m$, we approximate Eq. (2) by Eq. (2a)

$$f(\bar{b}) = \frac{\bar{b}}{\theta_1} \quad , \quad f'(\bar{b}) = \frac{1}{\theta_1} .$$

Substituting this into Eq. (22) yields

$$\lambda^\pm = \frac{pm}{\theta_1} - 1 \pm \frac{pm}{\theta_1} e^{-k^2 \sigma^2 / 2} . \quad (23)$$

For $m \ll \theta_1$, the term before the \pm symbol is negative. Instability, i.e., $\lambda > 0$, can therefore only be obtained for λ^+ . The largest contribution of the term following the \pm symbol in Eq. (23) is obtained when $e^{-k^2 \sigma^2 / 2}$ reaches its maximal value, which equals unity for $k = 0$. Hence we obtain as a sufficient condition for stability

$$\lambda^+ = \frac{2pm}{\theta_1} - 1 < 0 . \quad (24a)$$

This condition is equal to the requirement for stability of the virgin state to a uniform perturbation (i.e., Eq. (16a)) and is satisfied as long as the virgin state exists. We conclude that the virgin state is stable to both uniform and sinusoidal perturbations (see Table 1).

In the immune state, $\bar{b} = \frac{\theta_1}{p-1}$, we neglect m and approximate Eq. (2) by Eq. (2b), i.e.,

$$f(\bar{b}) = \frac{\bar{b}}{\theta_1 + \bar{b}} = \frac{1}{p} \quad \text{and} \quad f'(\bar{b}) = \frac{\theta_1}{(\theta_1 + \bar{b})^2} = \frac{(p-1)^2}{\theta_1 p^2} .$$

Hence Eq. (22) simplifies into

$$\lambda^\pm = \pm \frac{p-1}{p} e^{-k^2 \sigma^2 / 2} . \quad (24b)$$

Because $p > 1$, $\lambda^+ > 0$ and the immune state is unstable to sinusoidal perturbations. Substituting Eq. (21), $\lambda = \lambda^+$, $\beta_r \neq 0$ and $\beta_i = 0$, into Eq. (17) yields

$$b'(x, t) = e^{\lambda^+ t} \beta_r [e^{ikx} + e^{-ikx}] = 2\beta_r e^{\lambda^+ t} \cos kx ,$$

and hence destabilizing perturbations are of the form $\cos kx$ (see Table 1).

In the suppressed state, $\bar{b} = (p-1)\theta_2$, we neglect m and approximate Eq. (2) by Eq. (2c), i.e.,

$$f(\bar{b}) = \frac{\theta_2}{\theta_2 + \bar{b}} = \frac{1}{p} \quad \text{and} \quad f'(\bar{b}) = -\frac{\theta_2}{(\theta_2 + \bar{b})^2} = -\frac{1}{p^2 \theta_2} .$$

Hence Eq. (22) simplifies into

$$\lambda^\pm = \mp \frac{p-1}{p} e^{-k^2 \sigma^2 / 2} . \quad (24c)$$

Since $p > 1$, $\lambda^- > 0$ and the suppressed state is unstable to sinusoidal perturbations. Substituting Eq. (21), $\beta_r = 0$ and $\beta_i \neq 0$, into Eq. (17) yields

$$b'(x, t) = e^{\lambda^- t} \beta_i i [e^{ikx} - e^{-ikx}] = -2\beta_i e^{\lambda^- t} \sin kx ,$$

and hence destabilizing perturbations are of the form $\sin kx$ (see Table 1).

Sinusoidal perturbations of the immune state and suppressed state are expected to grow most rapidly when $\exp[-k^2\sigma^2/2] = 1$, i.e., for an infinite wavelength $k = 0$. The states differ however with respect to the form of the “most dangerous” sinusoidal perturbation, i.e., whether it is $\sin x$ or $\cos x$. It is important to realize that, with respect to $x = 0$, perturbations of the form $\sin x$ are asymmetric in the shape-space, whereas those of the form $\cos x$ are symmetric. Thus, if a perturbation of the form $\sin x$ increases certain populations around shape x , the complementary shapes around $-x$ decrease. Because these complementary shapes comprise the field $h(x)$, perturbations of the form $\sin x$ induce an opposite change in each population and its field. Conversely, since perturbations of the form $\cos x$ are symmetric around $x = 0$, cosinusoidal perturbations causes both populations and fields to change in the same direction.

For the immune state, in which $\cos kx$ is most dangerous, this means that any increased population gains an increased field. Indeed, by Eq. (2b), this causes the increased populations to increase further. Similarly, any decreased population will decrease. Additionally, as $k \rightarrow 0$, a $\cos kx$ perturbation, tends to increase all shapes uniformly. Indeed, the requirement for stability to sinusoidal perturbations Eq. (24b) is identical to that for stability to uniform perturbations Eq. (16b).

For the suppressed state, in which the asymmetric perturbation $\sin kx$ is destabilizing, this means that any increased population gains a decreased field. Indeed, by Eq. (2c), this causes the increased populations to increase further. Similarly, any decreased population will decrease. Additionally, as $k \rightarrow 0$, $\sin kx$, perturbs all shapes of equal sign in the same direction. Thus, one side of the shape-space populations increases, while on the other side populations decrease. Since the changes on the positive side of the shape-space will reinforce the rate of change on the negative side of shape-space, and vice-versa, such a perturbation grows rapidly.

A Discrete One-dimensional shape-space

So far in our analysis we have treated shape-space as if it were continuous. In order to numerically solve Eqs. (1)-(5) that determine our model we need to discretize the problem. Although this can be done with any of a number of well-studied procedures, we prefer to describe a discrete formulation of our model that can stand on its own as an immune network model. This is the same philosophy that underlies the numerical work in Segel & Perelson (1988) and Perelson & Segel (1991).

In the discrete formulation of the one-dimensional problem, the shape-space is divided into subintervals of width Δ . Let $b_i(t)$ represent the population size of a set of clones of related shape centered around $b(x, t)$, where $x = i\Delta$, $i = -N, \dots, N$. Let the interval of shapes represented by b_i be symmetrically distributed around $b(x, t)$, i.e., have width $\Delta/2$ on each side of $b(x, t)$. Thus the entire shape-space is now defined on $-L - \Delta/2 \leq x \leq L + \Delta/2$. Since there are $2N + 1$ intervals each of width Δ , $L = N\Delta$. If periodic boundary conditions are used, then the extension of shape-space beyond L is not needed. In this

case, we set $b_{-N} = b_N$ and hence we map the region of width $\Delta/2$ to the left of $-L$ into the region of width $\Delta/2$ to the left of L , and similarly for the regions to the right of L and $-L$. Despite the apparent complexity, we choose this symmetric representation so that b_0 represents clones distributed around the origin of shape-space.

In the discrete representation,

$$b_i(t) = b(x, t)\Delta, \quad i = -N, \dots, N,$$

where $b(x, t)$ is a density having units of number/unit length of shape, whereas b_i has units of number. In this formulation we can either view the b_i as representing "superclones", i.e., a set of clones of sufficiently similar shape that their behavior can not be distinguished, or if we have a fine enough grid as the set of all possible clones in the animal.

We now construct a set of discrete equations that are the counterparts of Eqs. (1)-(5). Thus

$$\frac{db_i}{dt} = m_i + b_i(pf(h_i) - 1), \quad (1')$$

where m_i is the rate of supply of clones of type i . The activation function $f(\cdot)$ is still given by Eq. (2). The counterpart of Eq. (3) specifying the field is

$$h_i = \sum_{j=-N}^N g(i, j)b_j(t)\Delta. \quad (3')$$

Because we have discretized shape-space, the Gaussian now becomes

$$g(i, j) = G(2\pi\sigma^2)^{-1/2} \exp[-(i + j)^2\Delta^2/2\sigma^2]. \quad (4')$$

If periodic boundary conditions are used, $b_{-N} = b_N$, this system forms a set of $2N$ ordinary differential equations. We use periodic boundary conditions to simulate having an infinite domain. Thus if the tails of the Gaussian reach the boundaries we wrap them around the domain, allowing the distance in the Gaussian to increase. Thus the field becomes

$$h_i = \sum_{j=-i-N}^{i+N} g(i, j)b_j(t)\Delta, \quad (3'')$$

where b_j is assumed to be $2N$ periodic, i.e., $b_j = b_{j+2N} = b_{j-2N}$.

In the discrete approach one can view this set of differential equations as forming the true model, which describes the interactions among a set of $2N$ clones. The continuous system of partial differential equations then is an approximate description and presumably a good one when N is large. The alternative approach is to view the partial differential equations as the true model. Then any of a number of discretizations are possible, some more accurate than the simple trapezoidal rule approximation for the integral in Eq. (3').

Simulation. We have simulated the discrete model by numerical integration. Since the space is sampled according to the Gaussian function $g(\cdot)$, and because Δ defines the step

size in space, we define $\Delta = \sigma/n$, where n is the number of intervals used to approximate one standard deviation of the Gaussian. We typically choose $n = 5$, and test the accuracy of the approximation by increasing n , which should not affect the results. For the size, $L = N\Delta$, of the shape-space we arbitrarily choose $L = 1$. The number of differential equations needed, $2N$, is then determined by $N = L/\Delta = nL/\sigma$. Increasing the accuracy of the spatial approximation, i.e., increasing n , thus increases the number of differential equations. To see that L is arbitrary, notice that once N and n are specified, the ratio $N/n = L/\sigma$, hence L can be varied as long as σ is chosen appropriately.

In order to verify our analytic derivations, we have simulated this discrete system with periodic boundary conditions. See Fig. 2. In the numerical approximation the maximum wavelength is $2L$. Owing to the periodic boundary conditions the wave has to repeat itself beyond L and $-L$. First, for the virgin state, $\bar{b} = m$, we confirmed the stability to both uniform and sinusoidal perturbations (not shown). Second, for the immune state, a uniform perturbation that increases the population size of clones initially at the immune state, $\bar{b} = \theta_1$, causes all of the clones to increase in size until the suppressed state, $\bar{b} = \theta_2$, is attained. Conversely, a uniform negative perturbation that decreases the population size of all clones at the immune state, causes clones to decrease uniformly in size until the virgin state, $\bar{b} = m$, is attained (not shown).

Recall that the immune state is unstable to perturbations of the form $\cos kx$, whereas the suppressed state is unstable to perturbations of the form $\sin kx$. Fig. 2a shows that a perturbation of the immune state of the form $\sin x$ has the tendency to damp out. However, due to non-linear effects the network fails to return to the immune state, but attains the uniform virgin state. Fig. 2b shows a perturbation of the immune state of the form $\cos x$. The perturbation increases in amplitude, spreads, approaches the uniform suppressed state $\bar{b} = \theta_2$, from where it grows further in the form of $\sin x$. As predicted, the suppressed state was found stable to uniform perturbations. Fig. 2c shows the effects of a perturbation of the form $\sin x$ made to the suppressed state $\bar{b} = \theta_2$. The perturbation grows monotonically until non-linear effects come into play. Conversely, a perturbation of the form $\cos x$ decreases in amplitude (Fig. 2d). These observations confirm our analytic results.

The simulations displayed in Figs. 2b and 2c did not attain an equilibrium distribution. The simulations were terminated because the long term dynamic behavior of the model grew unrealistic since some of the populations grow very large by self-stimulation. This is illustrated in Fig. 3a, which displays the distribution of clones and fields at $t = 50$ that is attained by continuation of the simulation shown in Fig. 2c. Figure 3a displays two peaks of about 10^{11} cells, having a stimulatory field value. Closer inspection shows that the fields of each peak are comprised of the tails of the Gaussian centered around the shape complementary to that peak. In other words, the clones stimulate themselves. To see this, consider the effect of a single clone at $x = x_1$, where $x_1 > 0$ but near the origin. Thus, let

$$b(x) = \begin{cases} b_1, & \text{if } x = x_1; \\ 0, & \text{if } x \neq x_1. \end{cases}$$

Then, by Eq. (3),

$$h(y) = \int g(x + y)b(x)dx = b_1g(x_1 + y). \quad (25)$$

The field is maximal at $y = -x_1$ and falls towards zero as y approaches x_1 . If, at some value of y , $h(y) \approx \sqrt{\theta_1\theta_2}$ then a clone at y will be maximally stimulated. If this maximal stimulation occurs at $y = x_1$, then the clone at x_1 will stimulate itself maximally. Roughly speaking this will occur if x_1 is within a few standard deviations of the origin. More precisely, we require $b_1g(2x_1) \approx \sqrt{\theta_1\theta_2}$ or $x_1 = \sigma\sqrt{2\log(\eta)}/2$, where $\eta = b_1/\sqrt{2\pi\sigma^2\theta_1\theta_2}$. Notice that the larger b_1 the further from the origin that the clone can be located and still maximally stimulate itself.

This analysis shows that we expect that the clone near the origin $x = 0$ in Fig. 3a will stimulate itself. This self-stimulation makes sense because shapes of shape zero are supposed to match themselves. B cell clones that stimulate themselves have been discovered in mice and are called *autobodies* (Kang & Köhler, 1986). In our model a low affinity antibody can grow large enough to sustain its own proliferation, and — as a side effect — dominate a large proportion of the shape-space. The other peak in Fig. 3a stimulates itself due to the periodic boundary condition. This is unrealistic. In Fig. 3b we further continue the simulation, showing the B cell distribution at $t = 50, 100, 150, 200$. This shows that the peaks keep on increasing, moving further into the tail of the Gaussian distribution. The population levels are unrealistically high, and we end up (at $t = 200$), with a repertoire containing only two species. In Figs. 3c-d we repeat these simulations for a system having fixed, instead of periodic boundaries. We now only find the antibody peak, but its behavior in terms of increasing to extremely large populations is the same.

In reality shape-spaces are neither infinite nor periodic. Having confirmed our analytic derivations, which were done for an infinite domain, it seems more realistic to omit the periodic boundary conditions and assume fixed boundaries for our more exploratory numerical work. Fixed boundaries only affect the field of the clones close to the boundaries. For instance, in a uniform state, $b = \bar{b}$, the field of the clone in the middle still approximates $h = \bar{b}$, but shapes at the boundary have a field that is closer to $h = \bar{b}/2$ than to $h = \bar{b}$. This non-uniform distribution of the field destabilizes the uniform suppressed state $\bar{b} = (p - 1)\theta_2$. Because the suppressed state is unstable to sinusoidal perturbations, and because completely uniform perturbations are unrealistic anyway, this hardly changes the interpretation of our results.

Assuming fixed boundaries eliminates the possibility of self-stimulation via the edges of the shape-space, but fails to solve the problem raised by the antibodies centered around $x = 0$. The reason why a small degree of self stimulation causes populations to be so large can be understood by writing

$$\frac{db}{dt} = m + b(pf(\epsilon b) - 1), \quad (26a)$$

where b is an autobody of shape x_1 , $h = \epsilon b$ defines the degree of self stimulation, and from Eq. (25) $\epsilon = g(2x_1)$. In analogy with the derivation of the three uniform equilibrium states, i.e., Eqs. (8), (10), & (11), we now obtain

$$\bar{b} = m, \quad \bar{b} = \frac{\theta_1}{\epsilon(p-1)}, \quad \bar{b} = \frac{(p-1)\theta_2}{\epsilon},$$

for the virgin, the immune, and the suppressed state of the autobody, respectively. In analogy with the stability analysis for uniform perturbations, one can show that the virgin and the suppressed state are stable, and that the immune state is unstable. Thus we expect an autobody, once stimulated, to grow sufficiently large that it ultimately suppresses itself. The counterintuitive property of the self stimulation is that a decrease of the degree of self stimulation, ϵ , increases the equilibrium population in either the immune or suppressed states. Instead of interactions fading away at the tails of the Gaussian distributions they may become more pronounced! We consider this point further in the Discussion.

A simple solution to the problem of large population sizes is to incorporate a self-limiting term in the growth equation for each population. Thus, we multiply the maximum proliferation rate p by the density dependent function $r(b)$, so that Eq. (1) is replaced by

$$\frac{\partial b}{\partial t} = m + b(pf(h)r(b) - 1), \quad (26b)$$

where $r(b)$ is

$$r(b) = \frac{\theta_3}{\theta_3 + b}.$$

Instead of $r(b)$ a variety of other functions could be used. For example, Segel & Perelson (1988) suggested $e^{-\lambda b}$. The logistic type term, $(1 - b/b_{max})$, could also be used. We prefer $r(b)$ for two reasons. First, unlike the logistic term there is no strict maximum population size. Populations can get larger than θ_3 but not much larger. Thus the limit to population growth is somewhat elastic. This is more akin to what happens in the immune system, where the total number of lymphocytes is controlled but can still rise during infections. Additionally, because a logistic term allows for negative growth rates, it requires the assumption that above the maximum population size stimulated clones decay more rapidly than non-stimulated clones. This need not be the case in the immune system. As to the exponential term, it also gives rise to an elastic limit, but it has the disadvantage that to find the steady state population size one needs to solve a transcendental equation rather than a polynomial.

Incorporating the density dependent function $r(b)$ into the model will have no effect on the stability results as long as $r(b)$ only plays a role at population densities that are much larger than the three equilibrium states $\bar{b} = m$, $\bar{b} = \theta_1/(p-1)$, and $\bar{b} = (p-1)\theta_2$, respectively. The equilibrium value that is attained by a population, b , limited by the growth limitation only, i.e., for $f(h) \approx 1$, is

$$\frac{\theta_3}{\theta_3 + b} = \frac{1}{p}, \quad \text{hence,} \quad \bar{b} = (p-1)\theta_3,$$

which is of order θ_3 . Setting $\theta_3 \gg \theta_2 \gg \theta_1 \gg m$, ensures that $r(b) \approx 1$ in the virgin, immune and suppressed equilibrium states. Whenever $r(b) \approx 1$ it can be omitted from Eq. (26b), reducing it to Eq. (1), that we have used for the stability analysis.

One can also show formally that adding $r(b)$ to the model does not add new uniform equilibrium states. Considering a region where $r(b)$ plays a functional role, i.e., let \bar{b} a uniform B cell population of order θ_3 . Because $h = \bar{b} = \theta_3 \gg \theta_2 \gg \theta_1$,

$$\frac{h}{\theta_1 + h} \approx 1 \quad , \quad \text{and} \quad \frac{\theta_2}{\theta_2 + h} \approx 0 .$$

As a result, $f(h) \approx 0$. However, if $f(h) \approx 0$, Eq. (26a) reduces to

$$\frac{\partial b}{\partial t} \approx m - b ,$$

which has the virgin state, $\bar{b} = m$, as the only equilibrium solution. Since $m \ll \theta_1 \ll \theta_2 \ll \theta_3$, \bar{b} is not of order θ_3 , which contradicts our assumption. Hence, besides the virgin, immune and suppressed states, there is no additional uniform equilibrium in the region where $\bar{b} \gg \theta_2$.

Plasticity. In Fig. 4 we show the time evolution of a network incorporating the self-limitation $r(b)$ with $\theta_3 = 10^6$. The variance is equal to that studied in Figs. 2 & 3, i.e., $\sigma = 0.045$. As an non-uniform initial condition, we now assign to each population a value that is randomly distributed around the suppressed state with 10% standard deviation. The main difference with the results shown above is that an equilibrium distribution is attained. In the equilibrium some populations are close to the maximum θ_3 , while other populations attain values around the immune and suppressed states. As was to be expected, the autobody close to the origin $x = 0$ grows to the maximum level. One can calculate the affinity at which the autobody will be located. From Eq. (1''), in order to stimulate itself $\theta_1 < \epsilon \bar{b} < \theta_2$, and $\bar{b} \approx (p - 1)\theta_3$. Since maximal growth is attained at $\epsilon \bar{b} = \sqrt{\theta_1 \theta_2}$, the autobody population is expected to be centered around

$$\epsilon = \frac{\sqrt{\theta_1 \theta_2}}{(p - 1)\theta_3} ,$$

which for our parameters is $\epsilon = 10^3/10^6 = 10^{-3}$. Further, since $\epsilon = g(2x_1)$, we find for the parameters in Fig. 4, $x_1 = 0.095$.

In Fig. 5 we display a number of different equilibrium distributions as a function of the standard deviation σ . (Note that Δ and N vary with σ , but that this should not affect the results). The main result is that the smaller the variance the more peaks are there in the repertoire. Interestingly, we find an organization that goes beyond the level of individual peaks. We find clusters of clones that are all distributed around either the immune or the suppressed state. The size of the clusters is much larger than the width of the Gaussian. The entire cluster interacts with another cluster at the opposite part of the shape-space. We may thus speak of a cluster of idiotypes and a cluster of anti-idiotypes. If the idiotypic cluster is in the immune state, the anti-idiotypic cluster is in the suppressed state (and vice

versa). Within each cluster we find an array of peaks and valleys of clone sizes distributed around the average state. Clones in interacting clusters behave in a coordinated way. While the network is slowly attaining an equilibrium distribution, idiotypic and anti-idiotypic clusters oscillate as if they were two interacting antibody species (not shown).

We have noted earlier in the bit-string models that clones may organize into larger units that have similar properties in the network (De Boer & Perelson, 1991). The present results suggests that these clusters may be of any size (see e.g. Figs. 5a & 6). An interesting implication is that one should be able to formulate a model in terms of interactions between clusters of clones.

For $\sigma = 0.016$, we display in Fig. 6 two different equilibrium distributions. The only difference between Figs. 5a, 6a & 6b is the (random) initial condition. Varying only the random number seed used to generate the initial random distribution, we have simulated a total of ten of these networks. Each of these attained a different equilibrium repertoire. We conclude that the immune repertoire of this shape-space model has a high degree of plasticity. The immunological implication of this is that external influences, such as self or foreign antigens, may easily influence the repertoire of the network. One common feature of all the repertoires that are attained is the large antibody located around the origin of the shape-space.

Self antigens. Coutinho (1989) and Holmberg *et al.* (1989) argue that the interaction between the environment of self antigens and the developing immune network determines repertoire selection. Having such a plasticity in repertoire selection we postulate that it is indeed to be expected that self antigens will influence the selection of the network repertoire. Within the shape-space framework, any particular antigen will also have a shape x , where $-L \leq x \leq L$, and its concentration $a(x)$ will influence the field of complementary B cell clones. Complete incorporation of antigen would modify Eq. (3) into

$$h(x, b) = \int_{-L}^L g(x, \hat{x}) [b(\hat{x}, t) + a(\hat{x}, t)] d\hat{x}, \quad (27)$$

and would require an additional partial differential equation for a specifying antigen dynamics. For self antigens, which we expect to be present at constant concentration, $\partial a / \partial t = 0$, no new equation need be added. Further, self antigens are thought to induce tolerance or non-responsiveness in clones that recognize them (cf., Goodnow *et al.*, 1988). To model this, for any self antigen of shape x we tolerize clones of shapes in the range $(x - \sigma, x + \sigma)$. Clones within this region are deleted from the repertoire by omitting the source from the bone marrow (i.e., $m_x = 0$). Thus, tolerance induces holes of a width 2σ in the repertoire. In Figs. 6c and 6d we show the same networks with the same initial conditions as the ones shown in Figs. 6a and 6b, respectively, but in the presence of three self antigens located at $x = -0.20, 0.21, 0.33$. Because the repertoires in Figs. 6a,b differ from those in Figs. 6c,d, we conclude that the self antigens do influence repertoire selection. Depending on how the deleted clones fit in the repertoire, this difference may either be substantial, as between Figs. 6a and 6c, or may be minor, as between Figs. 6b

and 6d. Additionally, because the same three self antigens select the different repertoires in Figs. 6c-d, we conclude that even a self-referential repertoire may be sufficiently plastic to be able to reflect further environmental differences.

We have also studied the response to foreign antigens by implementing Eq. (27). If an antigen is introduced in a stimulatory concentration, and contains sufficiently many epitopes (i.e., different shapes), it modifies the repertoire (not shown). Coutinho's and Holmberg's view is that immune responses to antigens do not come from the network but stem from the clonally organized compartment of the immune system. We show below that some idiotypes remain functionally disconnected from the network. Such shapes may therefore account for an immune response typical of a clonally organized immune system. Interestingly, whenever perturbations by antigens modify the repertoire, the disconnected shapes may become functionally connected to the network. This may account for a form of memory (Coutinho, 1989; De Boer & Perelson, 1991).

Clonal organization. The question of whether or not the immune system combines a functional idiotypic network with a set of clones functionally disconnected from the network can be addressed by searching for regions in shape-space in which both the field and the B cell populations are small, indicating that B cells exist in the virgin state. Such cells would not be stimulated by the network and hence would be available to respond to antigen as perceived in the classical picture of clonal selection theory. Virgin regions exist in the repertoires shown in Figs. 2-6. They tend to be located adjacent to the high peaks (of order θ_3) in the repertoire. The mere existence of these "virgin" regions fails to provide a conclusive answer to our question about the organization of the immune system, because the virgin regions occupy only a small proportion of the shape-space. We believe this may be an artefact due to the low dimensionality of the shape-space. Below, this question will be addressed further with a 2D shape-space model.

Towards an Automaton Model

Above we have assumed that m is small, i.e., $m \ll \theta_1$. Here we make a more drastic assumption and simplify Eq. (1) by setting $m = 0$. Thus, B cell dynamics are governed by

$$\frac{1}{b} \frac{\partial b}{\partial t} = pf(h) - 1. \quad (28a)$$

Changing variables to $B = \ln b$, we obtain

$$\frac{\partial B}{\partial t} = pf(h) - 1, \quad (28b)$$

where for each shape x

$$h(x, B) = \int_{-L}^L g(x, \hat{x}) e^{B(\hat{x}, t)} d\hat{x}.$$

Changing to logarithmic variables has the advantage that the variation in the rate of increase of each population is now bounded between

$$-1 \leq \frac{\partial B}{\partial t} \leq p - 1 \approx 1 .$$

Since this significantly reduces the stiffness of the differential equation, Eq. (28a), we simplify Eq. (28b) into the mapping

$$B(t + 1) = B(t) + pf(h) - 1 , \quad (28c)$$

which is equivalent to using an Euler integration method with step size one.

Since changing from a one-dimensional shape-space to a two-dimensional shape-space does not affect the stability conditions, we study this system as a 2D lattice mapping with shape variables x and y that are integers, $-N \leq x, y \leq N$. We propose a circular shape-space, i.e., one that is bounded by $x^2 + y^2 < N^2$. The rationale for this is that shapes with extreme values of both x and y should be rare:

In two-dimensions, the mapping is

$$B(x, y, t + 1) = B(x, y, t) + pf(h(x, y, B)) - 1 , \quad (29)$$

where the field, $h(x, y, B)$, is

$$h(x, y, B) = \Delta^2 \sum_{i, j \in C(-x, -y)} g(i, j) e^{B(i, j, t)} ,$$

where $C(-x, -y) = \{i, j \mid (i + x)^2 + (j + y)^2 \leq n^2\}$ is the circle centered at $(-x, -y)$ with radius n . In computing $h(x, y)$ we assume fixed boundaries. The function $g(i, j)$ is the two-dimensional Gaussian

$$g(i, j) = (2\pi\sigma^2)^{-1} \exp[-\Delta^2(i^2 + j^2)/2\sigma^2] . \quad (30)$$

The effect of a source of novel cells from the bone marrow is re-implemented in this model by requiring that populations $B(x, y)$ never become smaller than zero (note that $B = 0$ corresponds to $b = 1$, i.e., to one B cell). Thus, the mapping, Eq. (29), is modified to

$$B(x, y, t + 1) = \max[0, B(x, y, t) + pf(h(x, y, B)) - 1] . \quad (31)$$

A cellular automaton. A general formalism for studying lattice models with finite states is cellular automata. By changing to integer states, and by proposing a simple next state function, we reformulate our 2D lattice mapping into a cellular automaton. The advantages are that (1) the formalism is very general, and (2) that the integer arithmetic is so much faster than real arithmetic that it should become feasible to study 3D shape-spaces.

To formulate the cellular automaton, we use instead of the biphasic function, $f(h)$, the simple window automaton defined previously by Neumann and Weisbuch (1991); i.e., whenever the field $h(x, y)$ falls within the window $\theta_1 \leq h(x, y) \leq \theta_2$, clone $B(x, y, t)$

increases, otherwise it decreases. Choosing a time scale such that in one time unit a clone increases or decreases a factor of e , we obtain the next state function

$$B(x, y, t + 1) = \begin{cases} B(x, y, t) + 1 & \text{if } \theta_1 \leq h(x, y) \leq \theta_2 ; \\ \max[0, B(x, y, t) - 1] & \text{otherwise .} \end{cases} \quad (32)$$

The only fixed point of this function is the virgin state $B(x, y, t + 1) = B(x, y, t) = 0$. In our simulations of the window automaton, we set $\theta_1 = \ln(10^2) \approx 4$, and $\theta_2 = \ln(10^4) \approx 9$.

In the window automaton model we define the field to be the integer sum of the (logarithmic) clone sizes weighted by a Gaussian function of the distance in shape-space

$$h(x, y) = \sum_{i, j \in C(-x, -y)} \max \left[0, B(i, j, t) - \Delta^2 \frac{(i^2 + j^2)}{\sigma^2} \right], \quad (33)$$

where $C(-x, -y)$ is the circle of radius n defined above, h is an integer, and where we again assume fixed boundaries. The radius n is naturally defined by the distance at which large clones no longer contribute to the field, i.e., when $B(i, j, t) - \Delta^2 \frac{i^2 + j^2}{\sigma^2} < 0$.

The 2D patterns obtained with the cellular automaton model are very similar to those presented in Figs. 7-9 of the 2D lattice mapping. Because we intend to compare the 1D shape-space with the 2D shape-space, we will only present results of the 2D lattice mapping in which $B(x, y, t)$ is a real number.

The 2D Lattice Mapping

The standard way of formulating a discrete time lattice model is to develop transition rules that depend on some finite (and usually local) neighborhood of each cell in the lattice. Since our model is defined in terms of an infinite Gaussian function, we introduce a cut-off point below which interactions are assumed negligible. To implement the cut-off, we truncate the 2D Gaussian so that terms with amplitude below 10^{-3} are set to zero. This implies that the field is non-zero only over a neighborhood of radius n . By Eq. (30) this radius depends on the parameters σ and Δ . The fact that we don't consider a standard local neighborhood, but instead the neighborhood around the cell having complementary coordinates, introduces non-locality in the lattice. The implication is that processes in one region in the lattice influence processes in other distant regions.

The introduction of an affinity cut-off seems realistic because interactions at affinities below $10^4 M^{-1}$ or $5 \times 10^4 M^{-1}$ do not seem to lead to B cell stimulation (Fish *et al.*, 1989; Riley & Klinman, 1986; Klinman, 1972). Additionally, we have seen in Eqs. (25) & (1'') that the minimal affinity ϵ limits the maximal size that each individual population can attain. Thus an affinity cut-off of $\epsilon = 10^{-3}$, defining the smallest possible self-stimulation, sets the maximum self-stimulatory population to roughly $\theta_2/\epsilon = 10^7$. Since the maximum population size and the minimum affinity are coupled this way, we seem to have two choices for preventing populations to grow extremely large. The most natural choice in the lattice mapping seems to be a finite neighborhood, the most natural choice in the discrete

approximation to the continuous PDE model seems to be the maximum population size. See Appendix 1 for some technical subtleties that arise because we have set $m = 0$.

We have studied the lattice mapping for $N = 50, \Delta = 0.02, (L = 1), p = 2, \theta_1 = 10^2, \theta_2 = 10^4$, and several values of σ . Figures 7-9 display the distribution of clone and field sizes that were attained after 500 time steps for $\sigma = 0.022, 0.031, 0.063$. The size of the neighborhood was $n = 4, 5, 8$ in these three cases, respectively. At $t = 0$ each square in the lattice was assigned a random value distributed around the maximum of the bell shaped function, i.e., $B = \ln \sqrt{\theta_1 \theta_2}$, with 10% standard deviation. At each location (x, y) the greyscale indicates the size of the clone $B(x, y)$ (i.e., the left panels) and the size of the field $\ln h(x, y)$ (i.e., the right panels). The greyscales displayed in Figs. 7-9 display roughly circular patterns. The patterns are reminiscent of those typically found in reaction-diffusion systems. Were we to use the standard square local neighborhood, instead of the circular Gaussian neighborhood used here, the patterns would be more rectangular. Interestingly, the pattern formation depends on the non-locality that is introduced by the complementary neighborhoods. If we change the neighborhood relation into the standard local neighborhood, we find no pattern at all. Conversely, if we assume complementarity in one direction, but a local neighborhood in the other direction, we find patterns that are very similar to the patterns shown in Figs. 7-9. Different matching rules in different directions allow different properties of the binding site to be expressed. The interpretation of complementarity would for instance be a geometrical fit; the interpretation of a local neighborhood would for instance be hydrophobicity. Other properties, such as charge, require other (non-local) neighbor relations.

The distributions of clone sizes and field values in Figs. 7-9 form landscapes of roughly circular hills and valleys. These patterns resemble the distributions of the 1D shape-space shown in Figs. 2-6 in a number of ways. First, the field patterns are wider and rounder than that of the clone patterns. Second, the ridges and hills in the 2D clone patterns correspond to the peaks and clusters in the 1D clone patterns. Superimposing the clone and the field distributions reveals that the large clones are typically located at intermediate field values, i.e., at values between θ_1 and θ_2 . Thus the dark ridges of large clones correspond to contour lines of intermediate height in the field landscape. Third, as the variance of the Gaussian is made smaller, more peaks and valleys appear. Thus, the scale of the pattern increases with σ .

The $t = 500$ distributions displayed in Figs. 7-9 are not in a steady state. To illustrate this, we show in Figs. 10a-d, how clone sizes at four points in the shape-space vary with time. As can clearly be seen, the clone sizes fluctuate over several orders of magnitude, and some points may remain empty (i.e., $B(x, y) = 0$) over considerable periods of time. The oscillatory behavior does not seem to depend on the variance σ^2 . Inspection of the global pattern as it evolves in time reveals that the landscape of hills and valleys changes slowly (not shown). Thus, although clone sizes change on a rapid time scale, the global pattern seems to be more conserved and changes on a slower time scale. The same is true

in the 1D shape-space. We have described how the clusters may oscillate for a long time without changing their location in space.

Clonal organization. In the 1D shape-space and in the 2D lattice mapping we have scored the number of shapes that have a field and a clone size that are smaller than $\theta_1/10$; we call these the “disconnected” clones. Such shapes are only poorly stimulated by the network, and correspond to clones that would behave according to the tenets of classical antigen-driven clonal selection theory (Burnet, 1959). As a function of σ , we plot in Fig. 11 the average percentage of disconnected clones in 1D (o) and in 2D (●) shape-spaces. For both the 1D and the 2D shape-space, *increasing σ increases the percentage of disconnected clones.* This may seem counterintuitive because an increase in σ , i.e., in cross-reactivity of each clone should increase the connectedness of the network. The explanation seems to be that increasing σ causes the scale of the patterns to increase. This creates large valleys where both clones and fields are small. Even more striking is the difference between the 1D and the 2D shape-space. Apparently, increasing the dimension of the space increases the scale of the patterns, and hence the percentage of disconnected clones. An extrapolation from Fig. 11 into a higher dimensional shape-space would predict that it should be possible to obtain a substantial percentage of disconnected clones. Whether this can get close to the 80-90% of disconnected clones that Coutinho (1989) and Holmberg *et al.* (1989) estimate remains unknown.

The effect of an increase in dimensionality is two-fold. First, for equal values of σ , a 2D shape-space has a higher percentage of disconnected clones. Second, comparing Fig. 5c with Fig. 8, for both of which $\sigma = 0.032$, the 2D shape-space seems to allow for more local peaks. Thus, if the number of local peaks were to correspond to the number of specificities in the repertoire, it would seem that the 2D shape-space allows for a higher value of σ . Fig. 11 suggests that this would increase the percentage of disconnected clones.

Discussion

We have modified our earlier partial differential equation shape-space model (Segel & Perelson, 1988) so as to take into account the bell-shaped B cell activation function that has characterized much of our recent network modeling (cf. De Boer, 1988; De Boer & Hogeweg, 1989a-c; De Boer *et al.*, 1990; De Boer & Perelson, 1991; Weisbuch *et al.*, 1990; Perelson & Weisbuch, 1991). Whereas the original Segel-Perelson model had only one uniform steady state, the virgin state, this model has three: virgin, immune and suppressed. We have argued previously (Segel & Perelson, 1988) that one important characteristic of the virgin state is that it be stable but not too stable. Stability is important so that small random perturbations do not excite the system. However, it should not be so stable that a large perturbation, say by antigen, leads to no appreciable response. For the current model, we have shown that the virgin state is stable to both uniform and sinusoidal perturbations. To keep the state from being too stable, requires setting the parameters of the system near

the stability boundary. This can easily be done by adjusting θ_1 , the threshold for activation in the bell-shaped function.

In addition to the virgin state, our model has immune and suppressed states that are sustained by network activity. We showed that homogeneous immune and suppressed states are unstable to sinusoidal perturbation. Thus the entire immune system can not remain in a homogeneous activated state. Perturbing the system from either the homogeneous immune or suppressed state leads to the formation of a pattern of activity in shape-space, with some clones, roughly speaking, immune, some suppressed and others virgin. The generation of pattern in this system does not rely upon short-range activation and long-range inhibition.

Segel and Perelson (1988) considered a model that was similar in many respects to the model considered here. The basic equation (1) was similar, but included two exponentials limiting the total number of B cells and the maximum clone size, respectively. Their definition of the field (corresponding to Eqs. (3) and (4)) was the same as those used here. Instead of using the biphasic function (2), Segel and Perelson (1988) treated activation a and suppression s separately. Different standard deviations σ_a and σ_s were used in calculating h_a and h_s . Segel and Perelson were seeking a reaction-diffusion type instability of the uniform state. Hence they assumed a long range inhibition and a short range activation ($\sigma_s > \sigma_a$), although later they showed that this assumption could be reversed and the effect would be the same (Segel & Perelson, 1990). It should be borne in mind, however, that the requirement of relatively long range inhibition in reaction-diffusion theory is a consequence of the effort to bring about instability to small perturbations at a “most dangerous” wave length that is positive. In particular “most dangerous” perturbations of infinite or zero wavelengths are regarded as unacceptable in reaction diffusion theory. The reason is that if linear theory predicts instability at an intermediate wavelength then one has a good idea of the pattern wavelength that in fact emerges from the nonlinear equations—without resorting to extremely demanding nonlinear calculations. Thus, one can without difficulty compare one’s predictions with observed patterns.

The situation is different in the present instance. Here a primary goal is not to predict observed instability patterns but rather is to arrange conditions so that the virgin state is stable but not too stable. Hence it is quite admissible to consider instabilities at zero or infinite wavelength in seeking the stability boundary. There is therefore no reason to restrict oneself to relatively long range inhibition, and indeed our model contains only a single “range”. Note that there is still a pattern that develops from the infinite wavelength instability of the suppressed state, a pattern that is determined by nonlinear effects.

In previous models in which antibodies or B cells were characterized as being in levels, Ab_1, Ab_2, \dots , where antibodies on level 1 are complementary to those on level 2, etc., we found that immune and suppressed states tend to alternate. For example, Ab_1 immune, Ab_2 suppressed, Ab_i virgin, $i = 3, 4, \dots$ was a possible (localized) steady state (Weisbuch *et al.*, 1990). Depending on network topology and parameter values, “percolating” states

could also occur in which the entire immune system is activated; e.g., Ab_1 immune, Ab_2 suppressed, Ab_3 immune, Ab_4 suppressed, etc. (De Boer & Hogeweg, 1989b). The characteristic of all these possible steady states is that clones in the immune state which have high population tend to suppress clones connected to them, but the suppressed clones settle at population levels sufficiently higher than virgin that they can sustain the activation of the immune clone. In our current model there is no *a priori* assignment of clones to levels, yet we still see that in patterns that form spontaneously clusters of immune clones will lie in regions of shape-space that are complementary to clusters of suppressed clones. This is not surprising since the bell-shaped activation function requires an immune clone to see a low field as generated by a suppressed population, and a suppressed clone to see a high field of the type generated by an immune clone. What is surprising is that we find localized regions of shape-space, of width much larger than the field sensed by any single clone, in which all clones are activated. Further, this region is complementary in shape to a region of roughly equal width in which all clones are suppressed (Fig. 6a). These higher order localized structures seem to be emergent properties of our model.

To further characterize patterns in shape-space we developed a 2D lattice mapping and a 2D cellular automaton. The results obtained with these 2D shape-spaces bear resemblance to recent results obtained by (Stewart & Varela, 1991) with a different 2D shape-space model. Technically however, the two models differ significantly. First, they consider only two complementary idio-type species, black and white, that interact whenever their distance in shape-space is sufficiently small. Second, their model neglects population dynamics, thus, rather than dealing with gray scales that indicate population sizes, clones are either present or absent. Clones are present if they receive a degree of stimulation that falls between two thresholds (that are comparable to our θ_1 and θ_2). Patterns evolve by the introduction of novel shapes from the bone marrow. Novel shapes are only incorporated if their field falls within the stimulation window. If they are incorporated they change the fields of nearby clones. This, in turn, can lead to the elimination of those clones having a field outside the window. The pattern is updated until a coherent field is found. In contrast, since our shape-space incorporates all possible shapes, we assume that new cells emerging from the bone marrow are not unique, and thus may be merged with one of the pre-existing populations. Thus, in our model pattern changes are driven by changes in population size, and not by the introduction of novel clones per se. Lastly, Stewart and Varela, use their model to describe a shape-space mechanism for self tolerance. In our opinion, however, the tolerance they find is not robust to the incorporation of clonal population dynamics of the type that they have used previously (Varela *et al.*, 1988; Stewart & Varela, 1990) and that we use in this paper. When we follow Stewart and Varela's procedure, and incorporate self antigens evoking a stimulatory field, we invariably observe infinite expansion of self-reactive clones.

Studying this simple model of idiotypic B cell proliferation we have been troubled by the problem that B cell populations grow extremely large to compensate for low-affinity interactions. Since interaction terms are typically of the form *affinity* × *concentration*, the effect may be realistic. Two properties of the model that are responsible for the extremely

large populations are unrealistic however. First, as we have argued above, we need an affinity cut-off to account for the fact that low affinity antibodies are unable to stimulate B cells, even at high concentrations. However, because affinities of IgG antibodies may vary over six orders of magnitude, our model would still allow populations to deviate six orders of magnitude. This remains unrealistic. Antibodies of type IgM, which tend to be found in early networks, typically are all of low affinity, e.g., $10^4 - 10^5 \text{ M}^{-1}$ and thus this discrepancy in population levels may not appear for IgM interactions. Second, and most important, these artificially high population levels are probably due to the fact that in our model stimulated B cells fail to stop proliferating. Experiments suggest that B cells at a maximum go through eight rounds of cell division (cf. Klinman *et al.*, 1984). Usually, activated B cells mature into plasma cells, which produce antibody but do not divide. If we were to incorporate into our model B cell maturation into a non-dividing end-stage cell, as has been done in earlier models (Bell, 1970, 1971; Perelson *et al.*, 1976, 1978), we would achieve a model in which the individual populations remain bounded. Such a model might not need the *ad hoc* population limitation that we have introduced here.

Whether or not the immune network is able to combine a fully connected network with a clonal organization of part of the repertoire is partly answered by the current shape-space analysis. We do find regions of the shape-space where the field is so low that clones remain virgin. Clones in these regions are capable of responding to foreign antigens according to the tenets of classical clonal selection theory. The low ratios between virgin and stimulated clones that we find seem to be at variance with the ratios reported in the empirical literature, i.e., 10-20% in the network and 80-90% disconnected clones. However, the results suggest that shape-spaces of higher dimension will support large scale patterns that contain a higher percentage of disconnected clones. This is to be addressed in future research.

Acknowledgements

Work performed under the auspices of the U.S. Department of Energy, and supported in part by NIH Grant AI 28433, the U.S.-Israel Binational Science Foundation Grant 89-00146, and by the Santa Fe Institute through their Theoretical Immunology Program. We thank Dr. John Stewart for discussing his work with Varela on their 2D shape-space formalism, and making their unpublished manuscript available to us.

Table 1. Stability properties of the uniform steady states

state	stability to perturbation		most dangerous perturbation
	uniform	sinusoidal	
Virgin	Stable	Stable	—
Immune	Unstable	Unstable	$\cos kx$
Suppressed	Stable	Unstable	$\sin kx$

Legends to the Figures

Figure 1. Graph of the bell-shaped proliferation function, $f(h)$ given by Eq. (2), versus the logarithm of the field h . Equilibria involving proliferation, i.e., the immune and suppressed state, are close to the intersections of $f(h)$ with the line $y = p/2$, see the text.

Figure 2. Development of sinusoidal perturbations to the uniform immune and the uniform suppressed state. Periodic boundary conditions with parameters: $m = 1, p = 2, \theta_1 = 10^2, \theta_2 = 10^4, L = 1, \sigma = 0.045, n = 5, \Delta = 0.009, N = 112$. The final distribution is shown as a heavy line. (a) A perturbation around the immune state, $\bar{b} = 100$, of the form $50 \sin x\pi/L$, where $-L \leq x \leq L$, damps out during the first few time steps. Because the increased populations decrease more rapidly than the decreased populations increase, the increased populations receive insufficient stimulation at the time they attain the immune state. Hence they decrease further, and the system finally attains the virgin state $\bar{b} = m$. (b) A perturbation around the immune state, $\bar{b} = 100$, of the form $10 \cos x\pi/L$, where $-L \leq x \leq L$, increases and spreads through the shape-space. In the middle region the uniform suppressed state is attained. The network leaves the suppressed state via a distribution of the form $\sin x$. (c) A perturbation around the suppressed state $\bar{b} = 10^4$, of the form $10 \sin x\pi/L$, where $-L \leq x \leq L$, grows rapidly. The network finally approaches a pattern with narrow but high peaks. (d) A perturbation around the suppressed state $\bar{b} = 10^4$, of the form $10 \cos x\pi/L$ where $-L \leq x \leq L$, damps out and returns to the uniform suppressed state.

Figure 3. The distribution of the B cell populations (light lines) and of the fields (heavy lines) that are attained long after a destabilizing perturbation ($b' = 10 \sin x\pi/L$) of the suppressed state. Periodic boundary conditions with parameters as in Fig. 2. (a) The distribution at $t = 50$ on a logarithmic scale ranging to 10^{12} cells. The two, unrealistically large, peaks are sustained through self-stimulation. The corresponding peaks in the fields reach the opposite part of the shape-space by crossing at $x = 0$ and $x = L$. The low affinity that is typical of the tail of the Gaussian distribution is counter balanced by a very large population size. (b) The time evolution of these spiky patterns on a logarithmic scale ranging to 10^{15} cells. The B cell distributions are displayed at $t = 50, 100, 150, 200$. (c) As Fig. 3a but for fixed boundary conditions. Now the shape-space is dominated by a single large peak, which is a low affinity antibody. (d) As Fig. 3b but for fixed boundary conditions.

Figure 4. Time evolution of a network with bounded population sizes and fixed boundaries. Parameters as in Fig. 2 except $\theta_3 = 10^6$. In the initial state populations are randomly distributed around θ_2 with 10% standard deviation.

Figure 5. The distributions of B cell population sizes and fields, for models with bounded population sizes and fixed boundaries, depend on the range of interaction in shape-space, i.e., σ . Parameters as in Fig. 2 except $\theta_3 = 10^6$. We display the equilibrium repertoire attained at $t = 1000$. (a) $\sigma = 0.016, \Delta = 0.003, N = 316$. (b) $\sigma = 0.022, \Delta = 0.004, N =$

224. (c) $\sigma = 0.032, \Delta = 0.006, N = 158$. (d) $\sigma = 0.045, \Delta = 0.009, N = 112$. We indicate the size of σ by a heavy horizontal line running from $-\sigma$ to σ at the top of the Figure.

Figure 6. Steady state distributions for the model studied in Fig. 5a, with bounded population sizes and fixed boundaries. Parameters as in Fig. 5 except $\sigma = 0.016, \Delta = 0.003, N = 316$. Figs. 5a, 6a and 6b differ only in the seed of the random number generator used to generate the initial population distribution. Figs. c and d show the same two networks with three self antigens located at $x = -0.20, 0.21, 0.33$ (arrows).

Figure 7. 2D patterns in the lattice mapping after 500 iterations. Parameters: $p = 2, \theta_1 = 10^2, \theta_2 = 10^4, L = 1, N = 50, \Delta = 0.02, \sigma = 0.022$. (a) clone sizes: black corresponds to $B = 20$, light grey corresponds to $B = 0$. (b) field sizes: black corresponds to $\ln h = 17$, white corresponds to $\ln h = 0$.

Figure 8. As Fig. 7, but $N = 50, \Delta = 0.02, \sigma = 0.032$. (a) clone sizes. (b) field sizes (here black corresponds to $\ln h = 16$).

Figure 9. As Fig. 7, but $N = 50, \Delta = 0.02, \sigma = 0.063$. (a) clone sizes. (b) field sizes (here black corresponds to $\ln h = 15$).

Figure 10. Dynamic changes in the sizes of clones located at $(N/2, N/2), (-N/2, N/2), (N/2, -N/2)$, and $(-N/2, -N/2)$ in the lattice mapping for various values of σ . (a) $\sigma = 0.016$. (b) $\sigma = 0.032$. (c) $\sigma = 0.045$. (d) $\sigma = 0.063$.

Figure 11. The average percentage of disconnected clones at $t = 500$ in 1D (o) and 2D (•) shape-spaces. Each • is the average of four 2D simulations, each o is the average of five 1D simulations.

Figure 12. The equilibrium populations in a 3D or 2D network (see Appendix 1) as a function of the source m . Parameters: $p = 2, \theta_1 = 10^2, \theta_2 = 10^4$. (a) In a 3D network the clone with the highest affinity disappears when $m = 0$. (b) In 2D networks both a high affinity, i.e., $J_{12} = J_{21} = 0, J_{23} = J_{32} = 1$ (heavy lines), and a low affinity interaction, i.e., $J_{12} = J_{21} = 0.5, J_{23} = J_{32} = 0$ (light lines), are hardly dependent on m .

Appendix 1.

To transform our differential equation model into a mapping we omitted the source of cells from the bone marrow, i.e. we set $m = 0$. Since the source was small in any case, i.e., $m \ll \theta_1$, this seems to be a reasonable assumption. However, simulating the differential equation model Eq. (1') for $m = 0$, gave us very different results from those shown in Fig. 5 for $m = 1$. Instead of having peaks centered around maxima of either θ_1 , θ_2 , or θ_3 , all peaks had a maximum of about θ_3 . Simulating a 2D lattice mapping in which we incorporated a maximum population size of $\ln \theta_3$, the only peaks that were attained were comprised of clones at $\ln \theta_3$.

We give two indications that setting $m = 0$ reduces the plasticity of the system because it eliminates steady state solutions. First, the virgin state normally at $\bar{b} = m$ collapses to the origin leading to the elimination of all virgin clones and solutions that depend on virgin clones to maintain other clones in a nonvirgin state. As an example, consider the possible steady states of the two species system

$$\frac{db_1}{dt} = m + b_1(pf(J_{11}b_1 + J_{12}b_2) - 1) = 0, \quad (A.1)$$

$$\frac{db_2}{dt} = m + b_2(pf(J_{12}b_1 + J_{22}b_2) - 1) = 0, \quad (A.2)$$

where we have set $J_{21} = J_{12}$. To determine the steady state, we substitute Eq. (2) for $f(h)$ into Eq. (A.1) and solve the resulting quadratic equation for b_2 . Substituting into Eq. (A.2), rearranging and squaring to remove radicals, we obtain a 12th order polynomial equation for the steady state value of b_1 . Setting $m = 0$ converts this polynomial into b_1^6 times a sixth order polynomial. Thus six solutions collapse into the trivial solution $b_1 = 0$ when $m=0$. This shows that one loses nontrivial solutions by eliminating the source.

Second, we numerically studied a similar system with three populations where the second species was connected to species one and three. The interaction matrix, J , was given by

$$J = \begin{pmatrix} 0 & 0.5 & 0 \\ 0.5 & 0 & 1 \\ 0 & 1 & 0 \end{pmatrix}.$$

Here the coupling between b_2 and b_3 is twice that of b_2 with b_1 . In the presence of a source term one of the equilibria of this system is an immune state of b_2 that is maintained by both b_1 and b_3 . For $m = 10$, we find $b_2 \approx 2\theta_2$, $b_1 \approx 2\theta_1$, and $b_3 \approx 0.5\theta_1$ (Fig. 12a). In order to suppress b_1 , b_2 needs to be of order $2\theta_2$, since at a suppressive steady state with $p = 2$

$$f(h_1) = \frac{\theta_2}{\theta_2 + 0.5b_2} = \frac{1}{p} = \frac{1}{2}.$$

Since $b_2 = 2\theta_2$ doubles the suppression on b_3 , b_3 attains a population size that is intermediate between the suppressed and the virgin state. Such an intermediate state can only exist if $m > 0$. This is illustrated in Fig. 12a, which shows the equilibrium population

levels of the three populations as a function of m . Decreasing m decreases b_3 until it disappears. Note that it is b_3 that is excluded, i.e., it is again the lowest affinity interaction that dominates.

For comparison, we show in Fig. 12b the same immune state in the absence of b_3 , for $J_{12} = J_{21} = 0.5$ (the light lines), and in the absence of b_1 , for $J_{23} = J_{32} = 1$ (the heavy lines).

These findings suggest that eliminating the source term may significantly reduce the number of equilibria. In particular the co-existence of several clones of different affinity around either the immune or the suppressed state may become unlikely. We are presently contemplating approaches that would enable us to generalize this suggested result.

References

- Amit, A. G., Mariuzza, R. A., Phillips, S. E. V. & Poljak, R. J. (1986). Three-dimensional structure of an antigen-antibody complex at 2.8 Å resolution. *Science*, **233**, 747-753.
- Bell, G. (1970). Mathematical model of clonal selection and antibody production. *J. Theoret. Biol.*, **29**, 191-232.
- Bell, G. (1971). Mathematical model of clonal selection and antibody production. II. *J. Theoret. Biol.*, **33**, 339-378.
- Burnet, F. M. (1959). *The Clonal Selection Theory of Acquired Immunity*. Cambridge University Press, London.
- Coutinho, A. (1989). Beyond clonal selection and network. *Immunol. Revs.*, **110**, 63-87.
- De Boer, R. J. (1983). GRIND: Great Integrator Differential Equations., Bioinformatics Group, University of Utrecht, The Netherlands.
- De Boer, R. J. (1988). Symmetric idiotypic networks: connectance and switching, stability, and suppression. In: *Theoretical Immunology*, Part Two, (A. S. Perelson, Ed.), pp. 265-289, *SFI Studies in the Science of Complexity*, Vol. III, Addison-Wesley, Redwood City, CA.
- De Boer, R. J. (1989). Poor repertoire selection in symmetric idiotypic network models. *Immunology Letters*, **22**, 101-112.
- De Boer, R. J. & Hogeweg, P. (1989a). Memory but no suppression in low-Dimensional symmetric idiotypic networks. *Bull. Math. Biol.*, **51**, 223-246.
- De Boer, R. J. & Hogeweg, P. (1989b). Unreasonable implications of reasonable idiotypic network assumptions. *Bull. Math. Biol.*, **51**, 381-408.
- De Boer, R. J. & Hogeweg, P. (1989c). Idiotypic network models incorporating T-B cell cooperation: the conditions for percolation. *J. Theor. Biol.*, **139**, 17-38.
- De Boer, R. J., Kevrekidis, I. G. & Perelson, A. S. (1990). A simple idiotypic network model with complex dynamics. *Chem. Eng. Sci.*, **45**, 2375-2382.
- De Boer, R. J. & Perelson, A. S. (1991). Size and connectivity as emergent properties of a developing immune network. *J. Theoret. Biol.*, (in press).
- Dembo, M. & Goldstein, B. (1978). Theory of equilibrium binding of symmetric bivalent haptens to cell surface antibody: Application to histamine release from basophils. *J. Immunol.*, **121**, 345-353.
- Farmer, J. D., Packard, N. H. & Perelson, A. S. (1986). The immune system, adaptation and machine learning. *Physica*, **22D**, 187-204.
- Fish, S. Zenowich, E., Fleming, M. & Manser, T. (1989) Molecular analysis of original antigenic sin. I. Clonal selection, somatic mutation, and isotype switching during a memory B cell response. *J. Exp. Med.*, **170**, 1191-1209.

- Goodnow, C. C., Crosbie, J., Adelstein, S., Lavoie, T. B., Smith-Gill, S. J., Brink, R. A., Pritchard-Briscoe, H., Wotherspon, J. S., Loblay, R. H., Raphael, K., Trent, R. J. and Basten, A. (1988). Altered immunoglobulin expression and functional silencing of self-reactive B lymphocytes in transgenic mice. *Nature*, **334**, 676-682.
- Holmberg, D., Freitas, A. A., Portnoi, D., Jacquemart, F. & Coutinho, A. (1986b). Antibody repertoires of normal BALB/c mice: B lymphocyte populations defined by state of activation. *Immunol. Revs.*, **93**, 147-169.
- Holmberg, D., Andersson, Å., Carlson, L. & Forsgen, S. (1989). Establishment and functional implications of B-cell connectivity. *Immunol. Rev.*, **110**, 89-103.
- Jerne, N. K. (1974). Towards a network theory of the immune system. *Ann. Immunol. (Inst. Pasteur)*, **125 C**, 373-389.
- Kang, C.-Y. & Köhler, H. (1986). A novel chimeric antibody with circular network characteristics: autobody. *Ann. N.Y. Acad. Sci.*, **475**, 114-122.
- Klinman, N. R., Press, J. L., Pickard, A. R., Woodland, R. T. & Dewey, A. F. (1974). Biography of the B cell. In: *The Immune System, Genes, Receptors, Signals*, Sercarz, E. E., Williamson, A. R. & Fox, C. F., eds. Academic Press, New York, pp. 357-365.
- Klinman, N. R. (1972). The mechanism of antigenic stimulation of primary and secondary clonal precursor cells. *J. Exp. Med.*, **136**, 241-260.
- Lundkvist, I., Coutinho, A., Varela, F. & Holmberg, D. (1989). Evidence for a functional idiotypic network amongst natural antibodies in normal mice. *Proc. Nat. Acad. Sci. USA.*, **86**, 5074-5078.
- Neumann, A.U. & Weisbuch, G (1991). Window automata analysis of population dynamics in the immune system. *Bull. Math. Biol.*, In press.
- Percus, J. (1988). Polydispersity in immune networks. In: *Theoretical Immunology*, (A. S. Perelson, Ed.), Part Two, pp. 345-358 *SFI Studies in the Science of Complexity*, Vol. III, Addison-Wesley, Redwood City, CA.
- Percus, J. (1989). Tree structures in immunology. In: *Applications of Combinatorics and Graph Theory to the Biological and Social Sciences*, (F. Roberts, Ed.), pp. 259-276, Springer-Verlag, New York.
- Pereira, P., Forni, L., Larsson, E. L., Cooper, M., Heusser, C. & Coutinho, A. (1986). Autonomous activation of B and T cells in antigen-free mice. *Eur. J. Immunol.*, **16**, 685-688.
- Perelson, A. S. (1984). Some Mathematical Models of Receptor Clustering by Multivalent Ligands. In: *Cell Surface Dynamics: Concepts and Models* (A. S. Perelson, DeLisi, C. & Wiegel, F. M., Eds.), pp. 223-276, Marcel Dekker, New York.
- Perelson, A. S. (1988). Towards a realistic model of the immune network. In: *Theoretical Immunology* (A. S. Perelson, Ed.), Part Two, pp. 377-401 *SFI Studies in the Science of Complexity*, Vol. III, Addison-Wesley, Redwood City, CA.
- Perelson, A. S. (1989a). Immune network theory. *Immunol. Rev.*, **110**, 5-36.

- Perelson, A. S. (1989b). Immune networks: a topological view. In: *Cell to Cell Signalling: From Experiments to Theoretical Models*, (A. Goldbeter, Ed.), pp. 261–262, Academic Press, London.
- Perelson, A. S. & Oster, G. F. (1979) Theoretical studies on clonal selection: minimal antibody repertoire size and reliability of self-non-self discrimination. *J. Theor. Biol.*, **81**, 645–670.
- Perelson, A. S. & DeLisi, C. (1980). Receptor clustering on a cell surface. I. Theory of receptor cross-linking by ligands bearing two chemically identical functional groups. *Math. Biosciences*, **48**, 71–110.
- Perelson, A. S., Mirmirani, M. & Oster, G. F. (1976). Optimal strategies in immunology, I. B-cell differentiation and proliferation. *J. Math. Biol.*, **3**, 325–367.
- Perelson, A. S., Mirmirani, M. & Oster, G. F. (1978). Optimal strategies in immunology, II. B memory cell production. *J. Math. Biol.*, **5**, 213–256.
- Perelson, A. S. & Segel, L. A. (1991). On the shape-space approach to the immune system: A B cell antibody model. *J. Stat. Phys.*, (in preparation).
- Perelson, A. S. & Weisbuch, G. (1991). Modeling immune reactivity in secondary lymphoid organs. *Bull. Math. Biol.*, (submitted).
- Press, W. H., Flannery, B. P., Teukolsky, S. A. & Vetterling, W. T. (1988). *Numerical Recipes in C. The Art of Scientific Computing*, Cambridge University Press, Cambridge.
- Riley, R. L. & Klinman, N. R. (1986). The affinity threshold for antigenic triggering differs for tolerance susceptible immature precursors vs mature primary B cells. *J. Immunol.*, **136**, 3147–3154.
- Segel, L. A. & Perelson, A. S. (1988). Computations in shape-space: a new approach to immune network theory. In: *Theoretical Immunology* (A. S. Perelson, Ed.), Part Two, pp. 321–343 *SFI Studies in the Science of Complexity*, Vol. III, Addison-Wesley, Redwood City, CA.
- Segel, L. A. & Perelson, A. S. (1989). shape-space analysis of immune networks. In: *Cell to Cell Signalling: From Experiments to Theoretical Models*, (A. Goldbeter, Ed.), pp. 273–283, Academic Press, New York.
- Segel, L. A. & Perelson, A. S. (1990). A paradoxical instability caused by relatively short range inhibition. *Siam J. Appl. Math.*, **50**, 91–107.
- Sheriff, S., Silverton, E. W., Padlan, E. A., Cohen, G. H., Smith-Gill, S. J., Finzel, B. C. & Davies, D. R. (1987). Three-dimensional structure of an antibody-antigen complex. *Science*, **84**, 8075–8079.
- Stanfield, R. L., Fieser, T. M., Lerner, R. A. & Wilson, I. A. (1990). Crystal structures of an antibody to a peptide and its complex with peptide antigen at 2.8 Å. *Science*, **248**, 712–719.

- Stewart, J. & Varela, F.J. (1990). Dynamics of a class of immune networks. II. Oscillatory activity of cellular and humoral components. *J. Theor. Biol.*, 144, 103–115.
- Stewart, J & Varela, F.J. (1991). Morphogenesis in shape-space. Elementary meta-dynamics in a model of the immune network. *J. Theor. Biol.*, Submitted.
- Varela, F.J., Coutinho, A., Dupire, B. & Vaz, N.N. (1988). Cognitive networks: immune, neural, and otherwise. In: *Theoretical Immunology*, Part Two, (A.S. Perelson, Ed.), pp. 359–375, *SFI Studies in the Science of Complexity*, Vol. III, Addison-Wesley, Redwood City, CA.
- Weinand, R. G. (1990). Somatic mutation, affinity maturation and the antibody repertoire: a computer model. *J. Theor. Biol.*, 143, 343–382.
- Weinand, R. G. (1991). Somatic mutation and the antibody repertoire: A computational model of shape-space. In: *Molecular Evolution on Rugged Landscapes*, (A. S. Perelson and S. A. Kauffman, Eds.), pp. 215–236, *SFI Studies in the Science of Complexity*, Vol. IX, Addison-Wesley, Redwood City, CA.
- Weisbuch, G. (1990). A shape space approach to the dynamics of the immune system. *J. Theor Biol.*, 143, 507–522.
- Weisbuch, G., De Boer, R. J. & Perelson, A. S. (1990). Localized memories in idiotypic networks. *J. Theor. Biol.*, 146, 483–499.

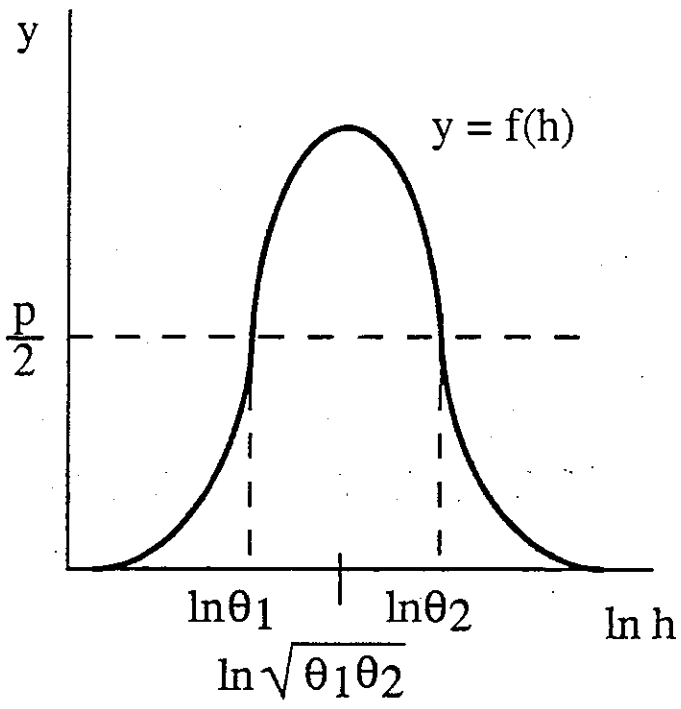


Fig. 1

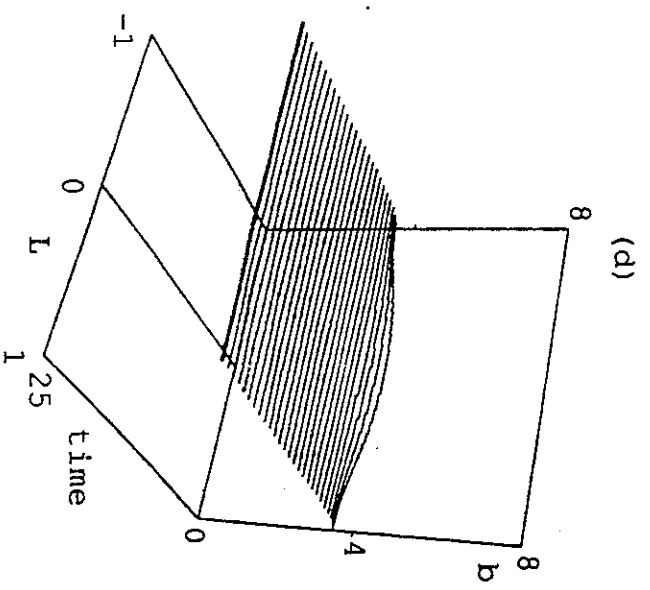
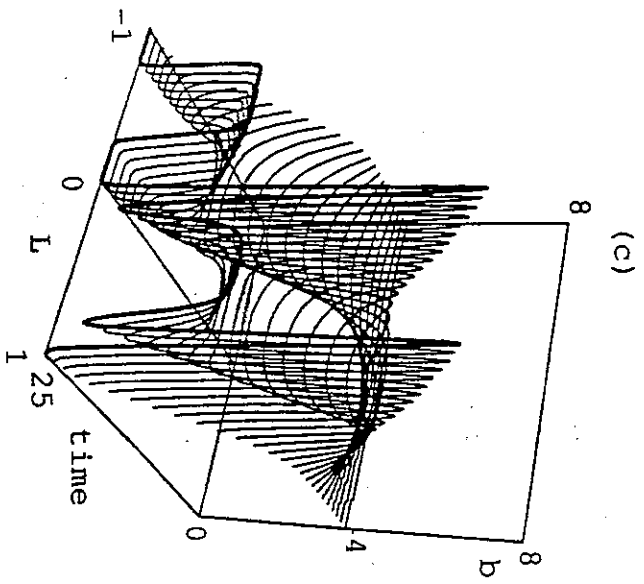
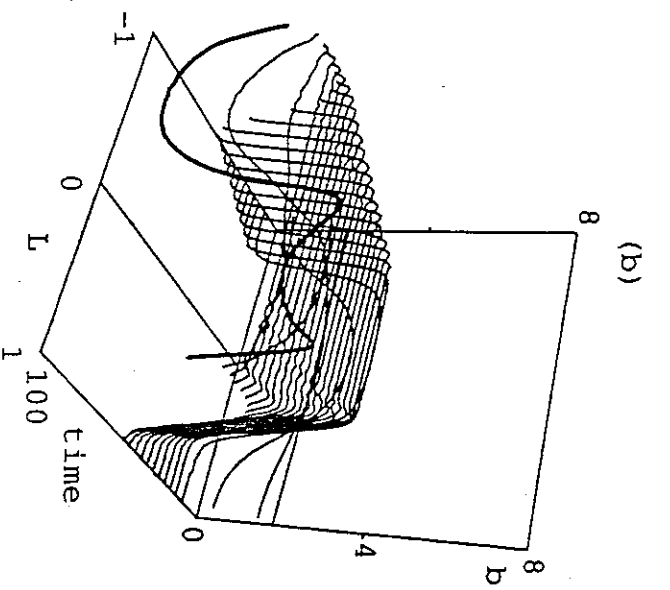
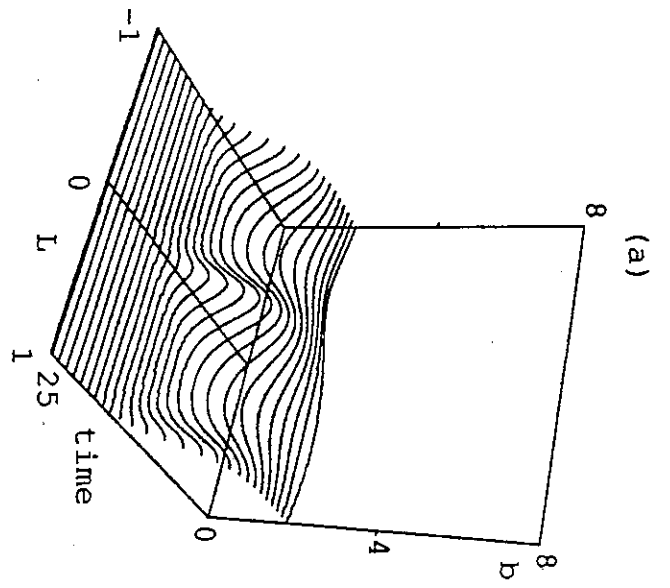


Fig. 2

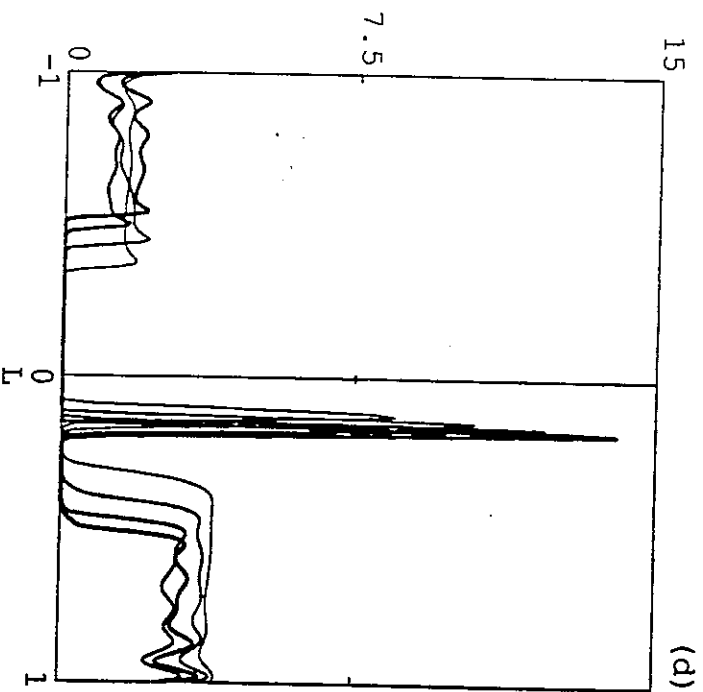
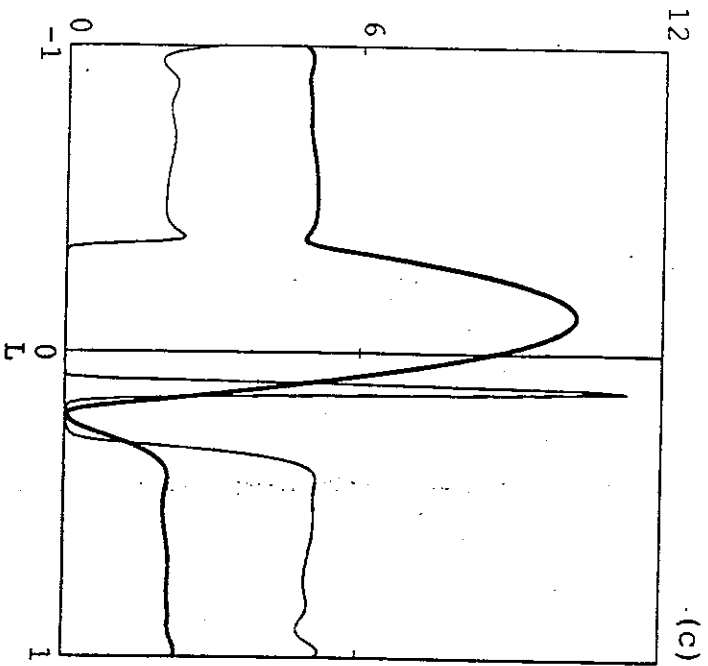
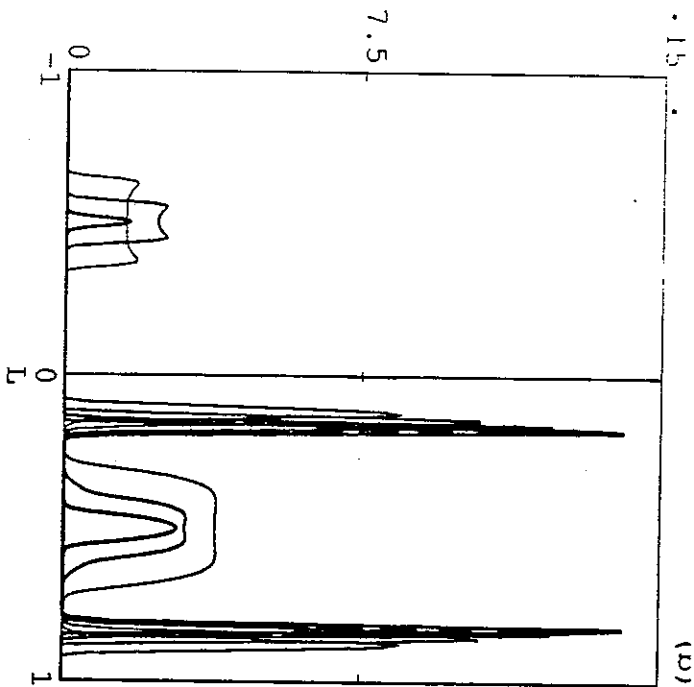
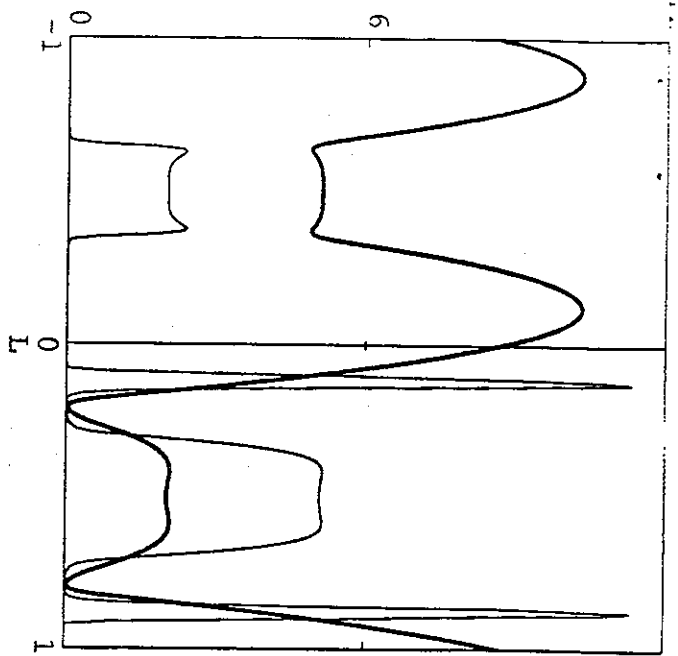
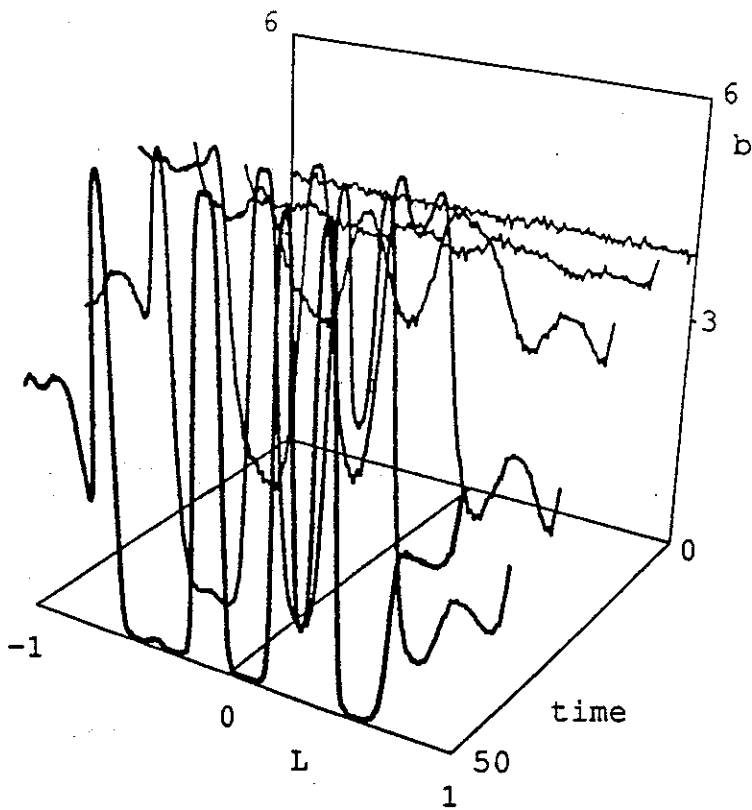


Fig. 3

Fig. 4



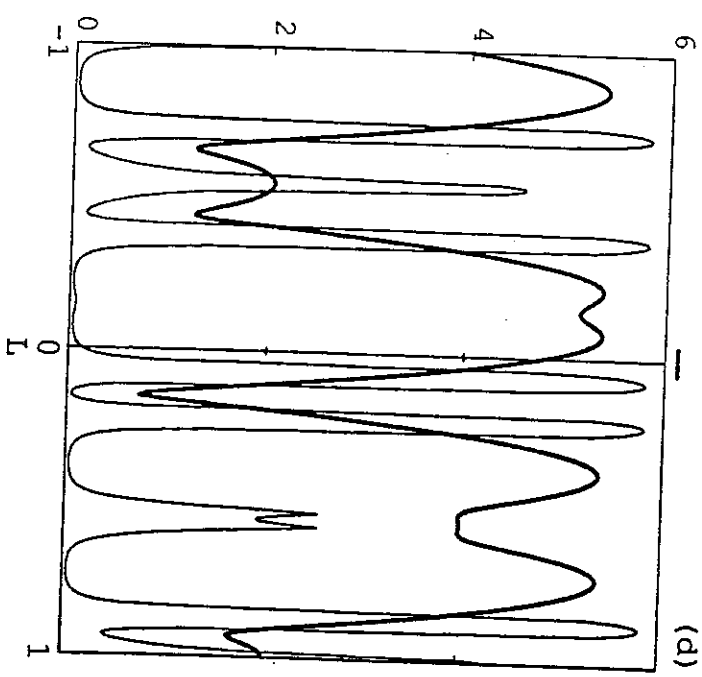
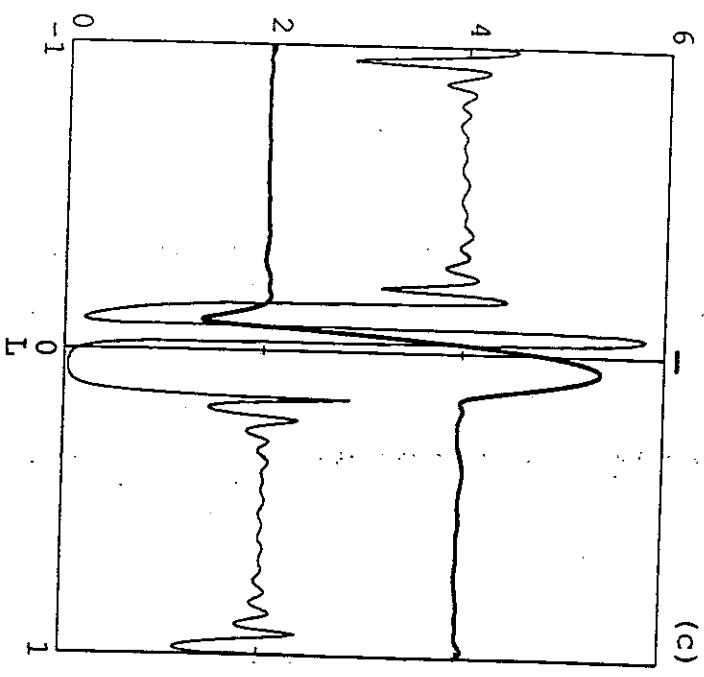
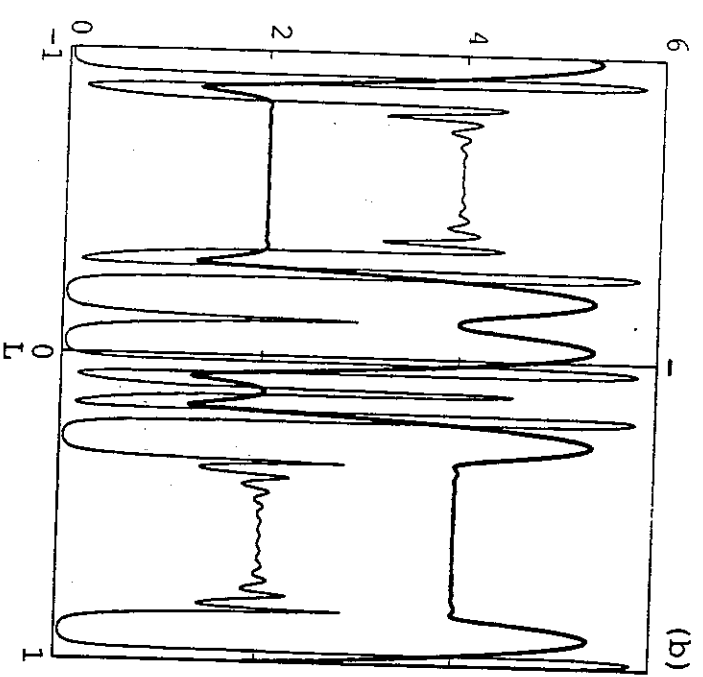
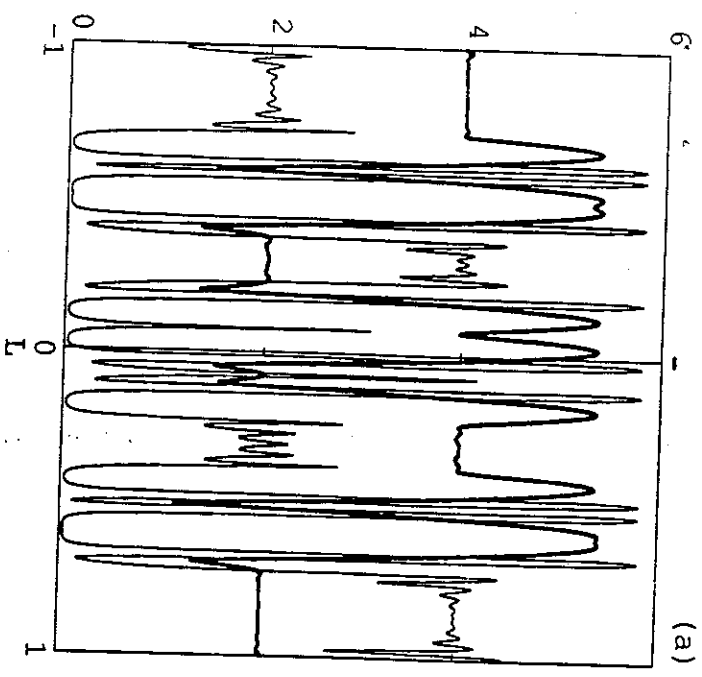


Fig. 5

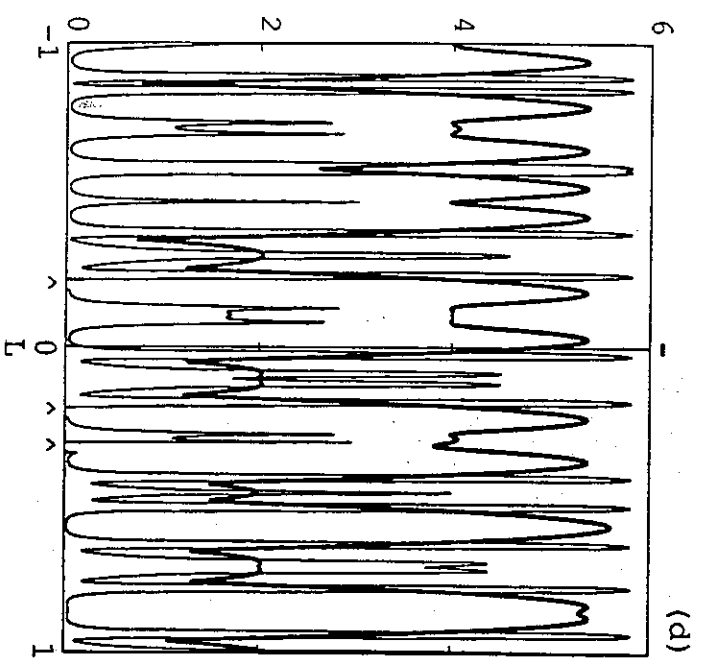
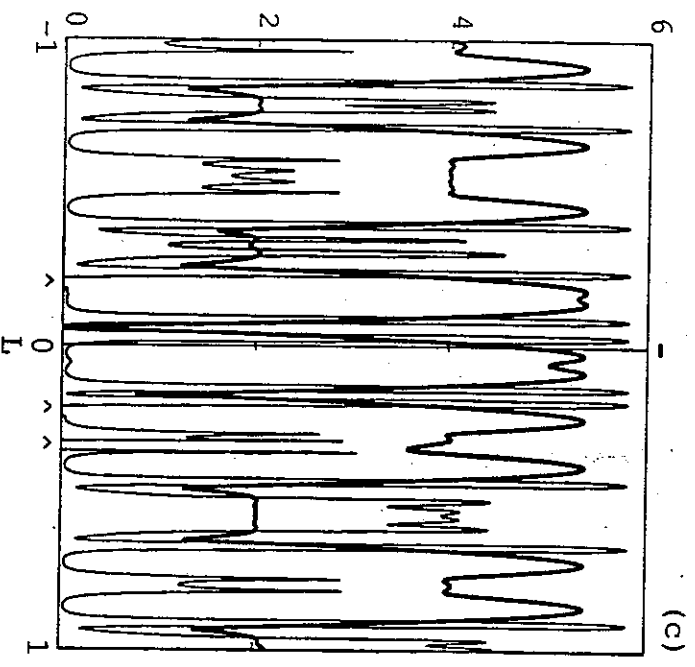
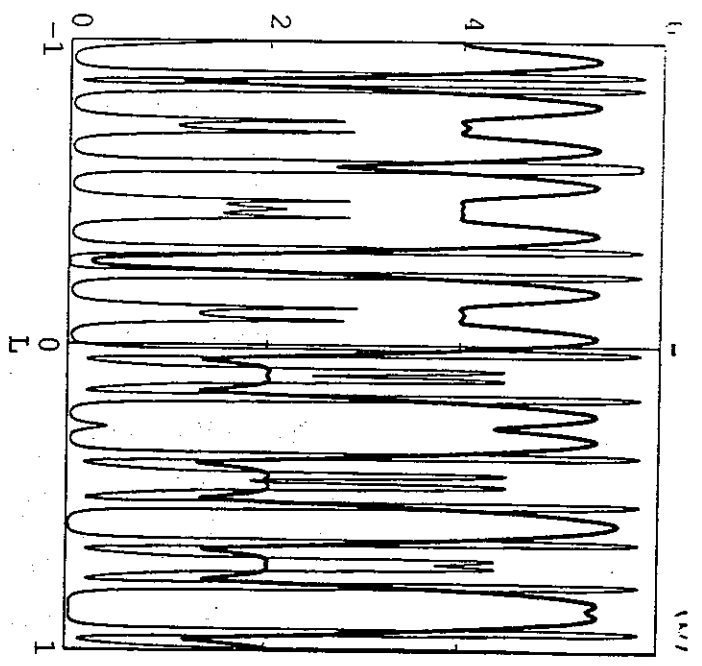
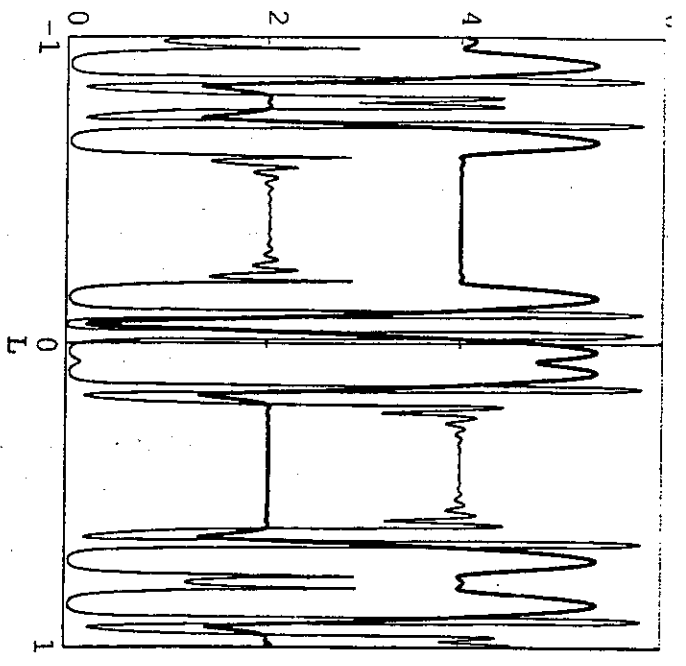
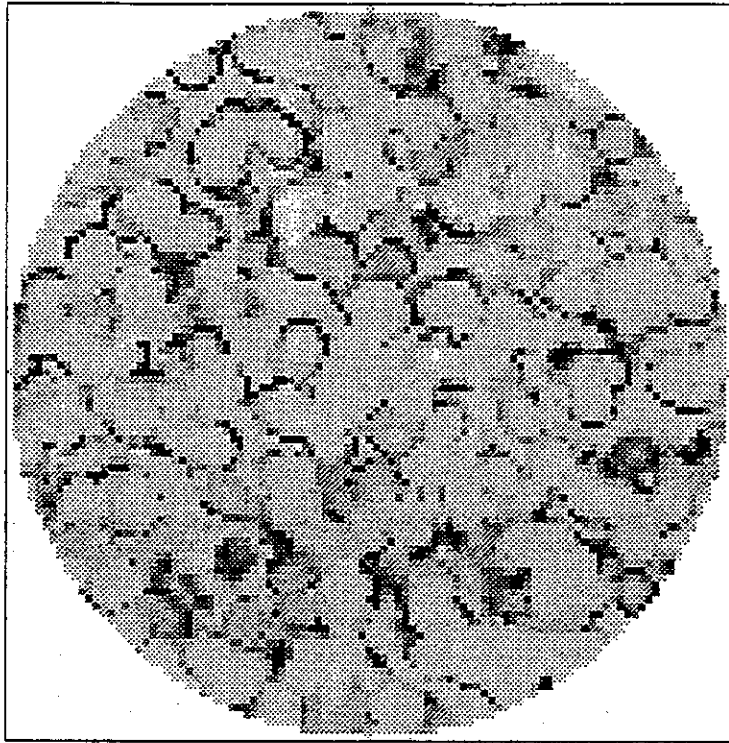
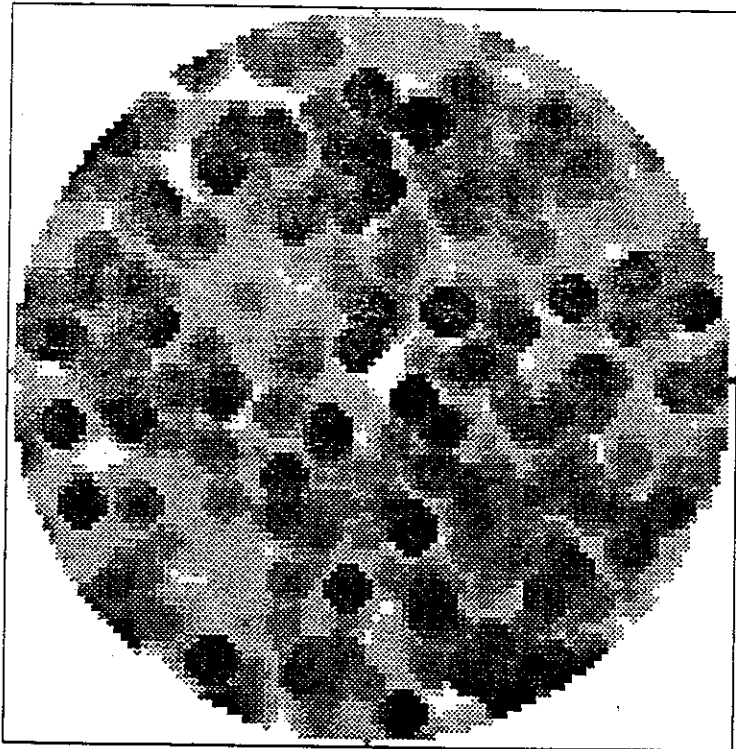


Fig. 6

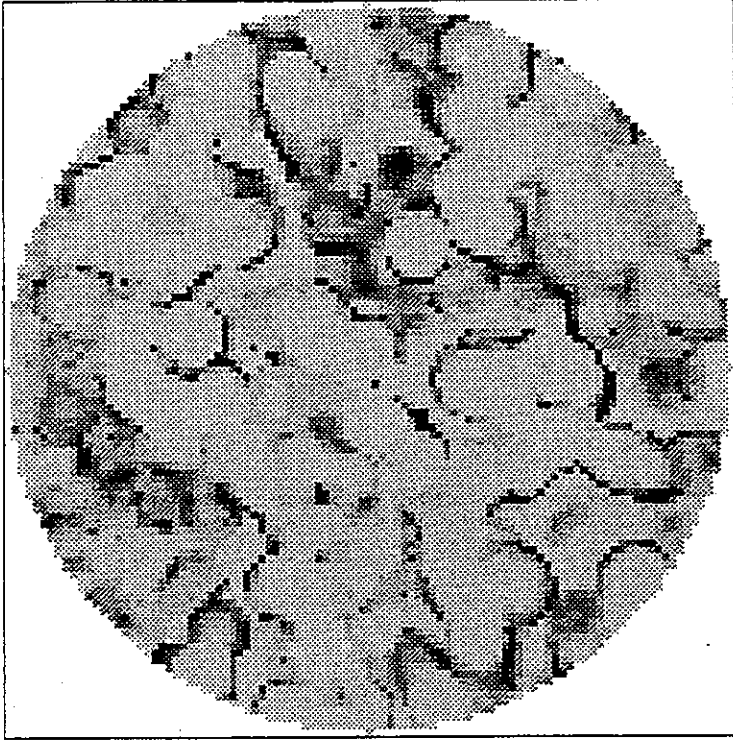


(a)

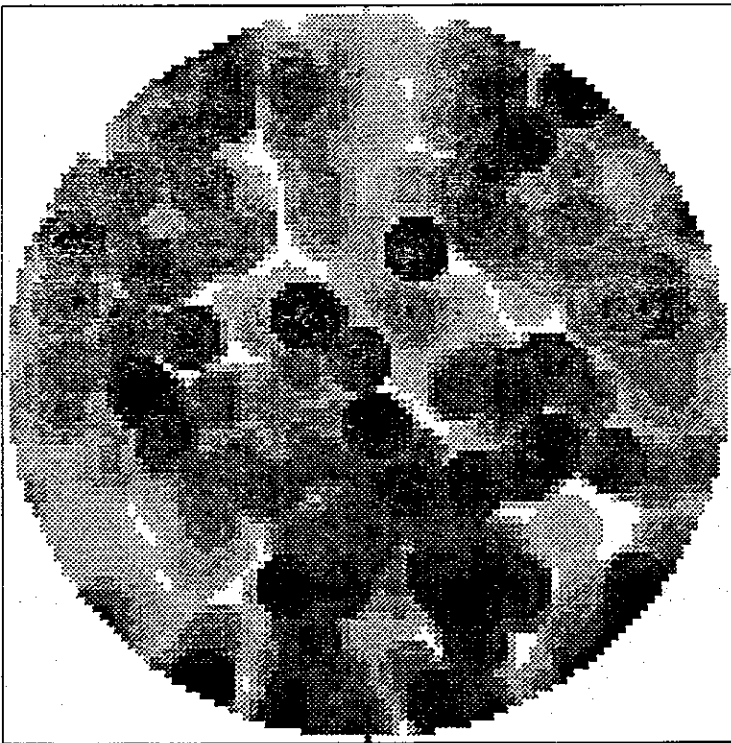


(b)

Fig. 7

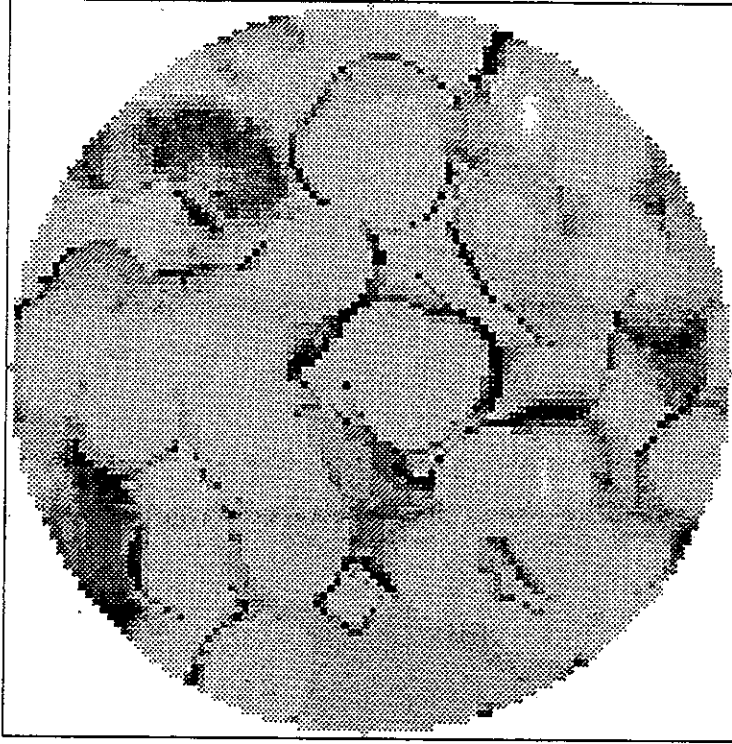


(a)

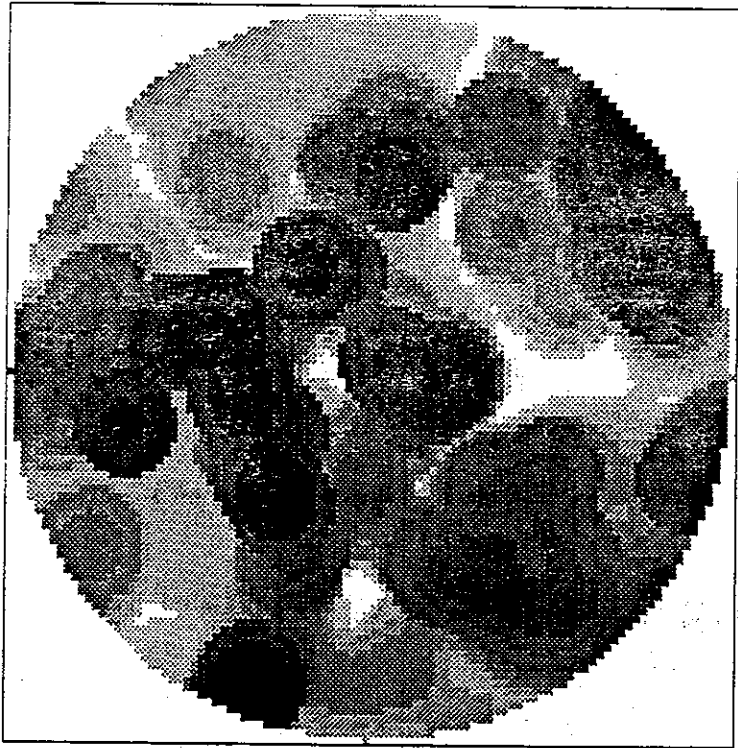


(b)

Fig. 8



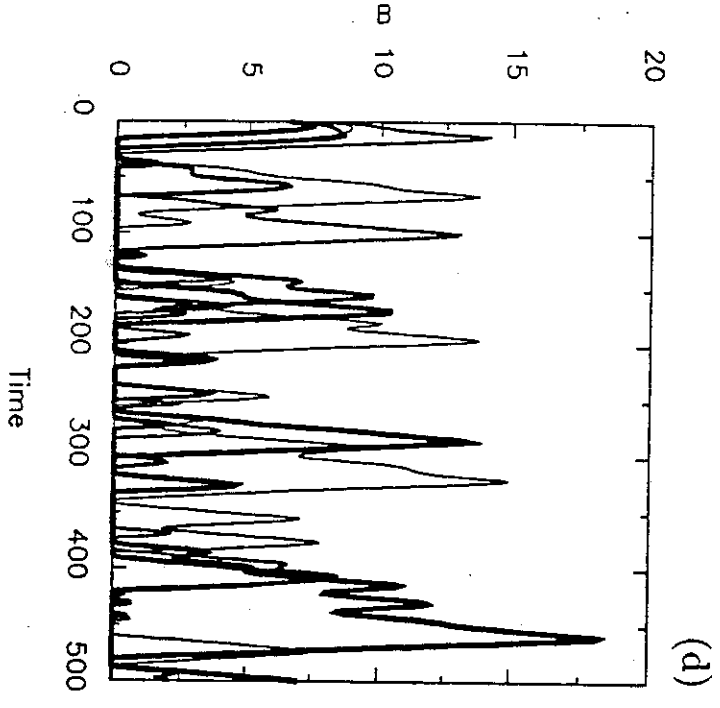
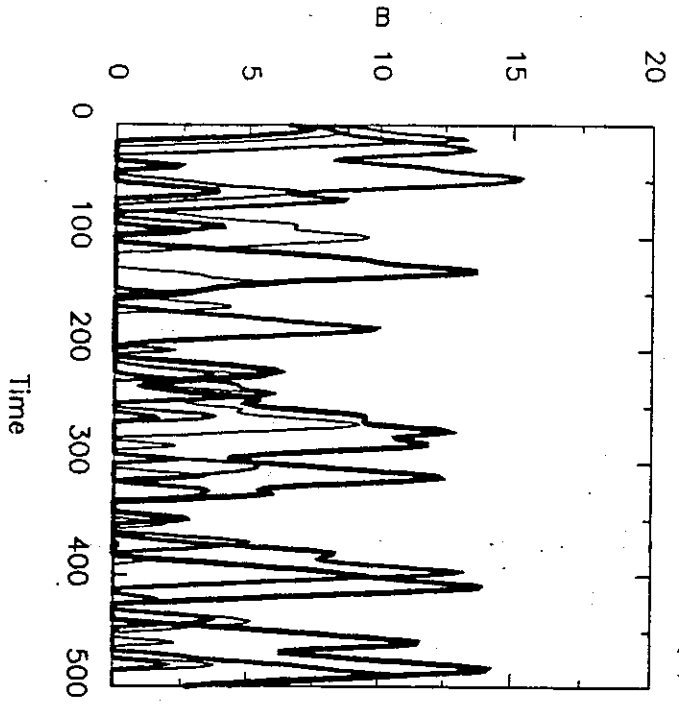
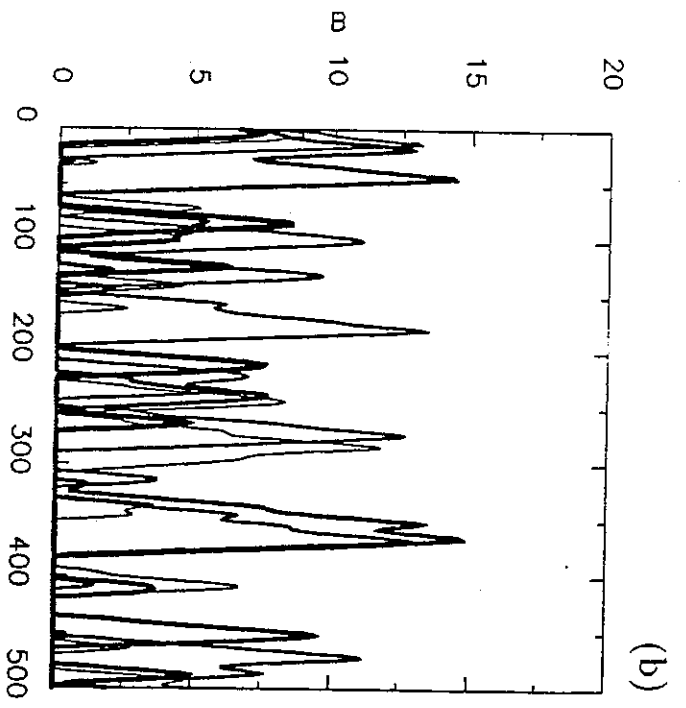
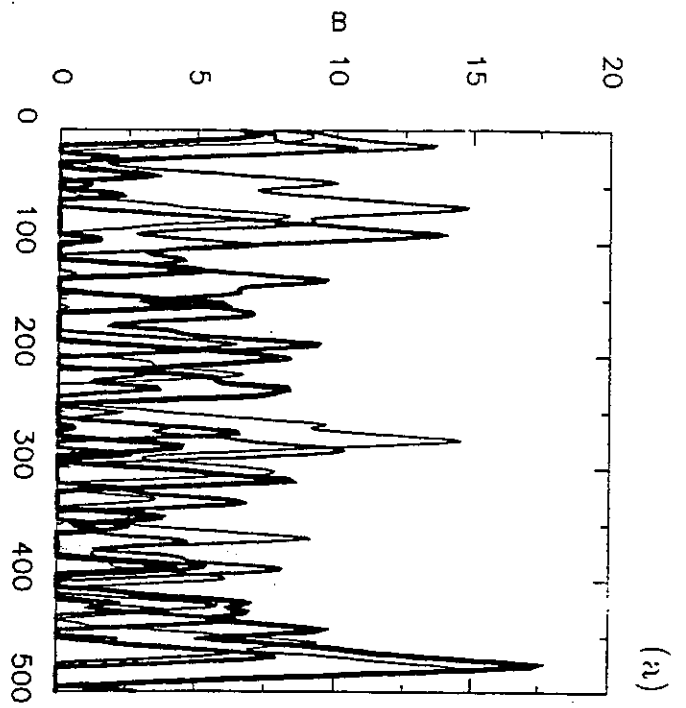
(a)



(b)

Fig. 9

Fig. 10



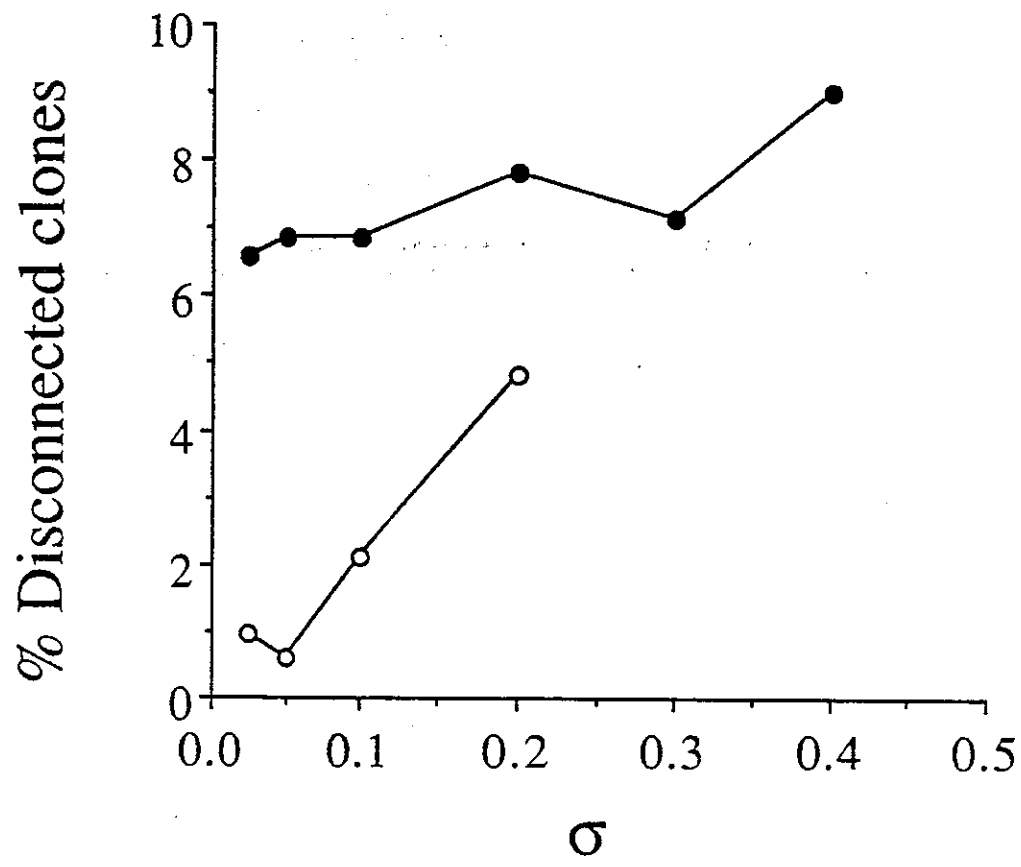


Fig. 11

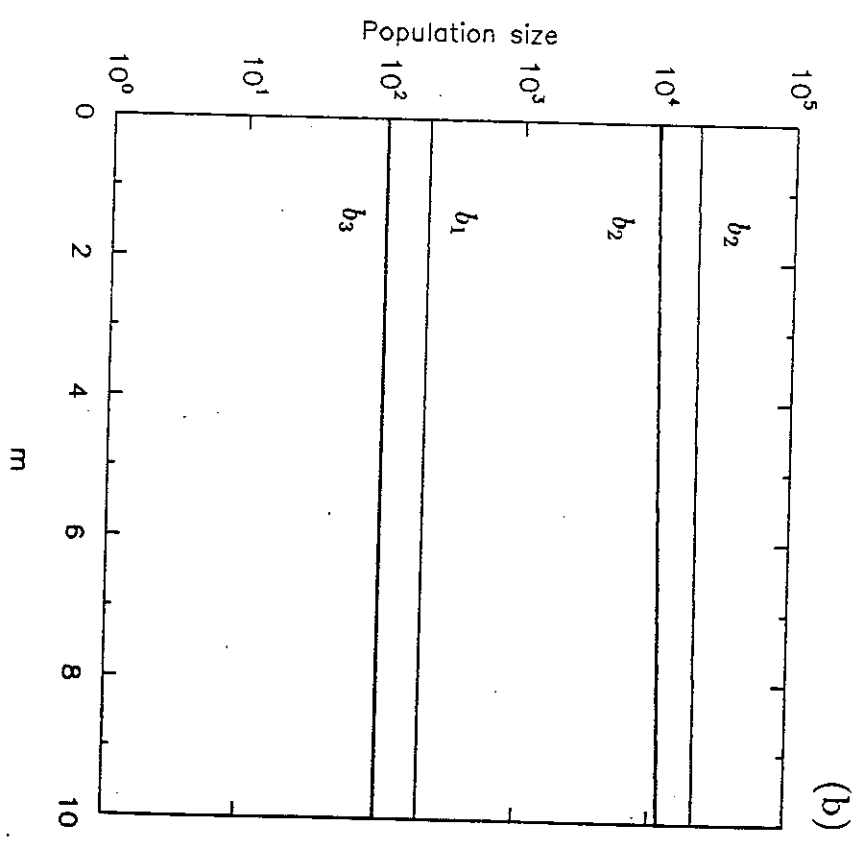
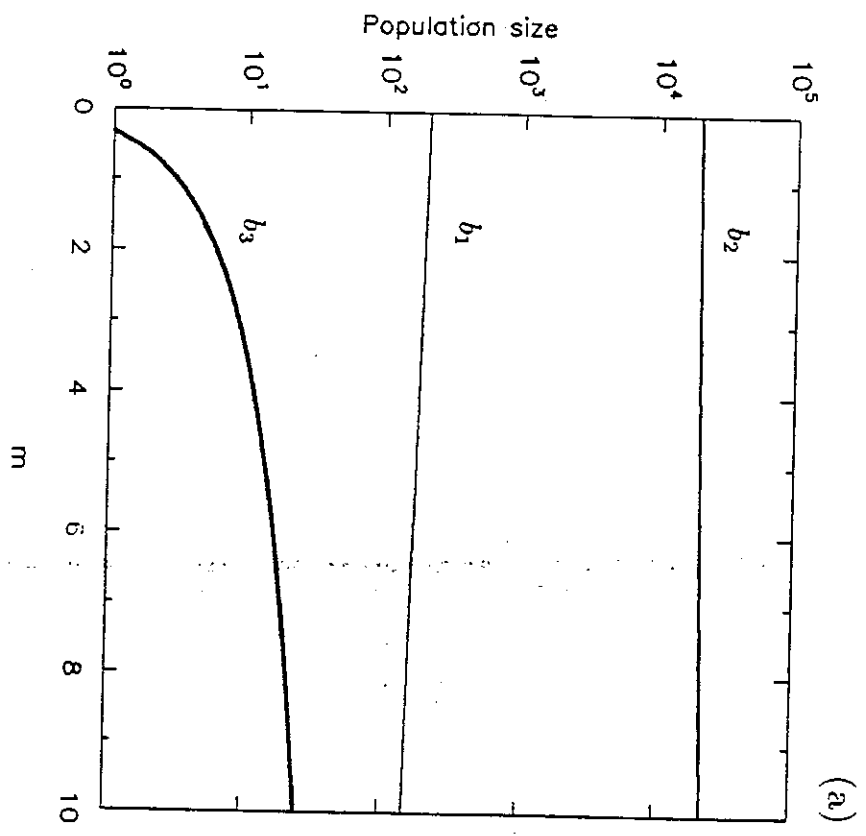
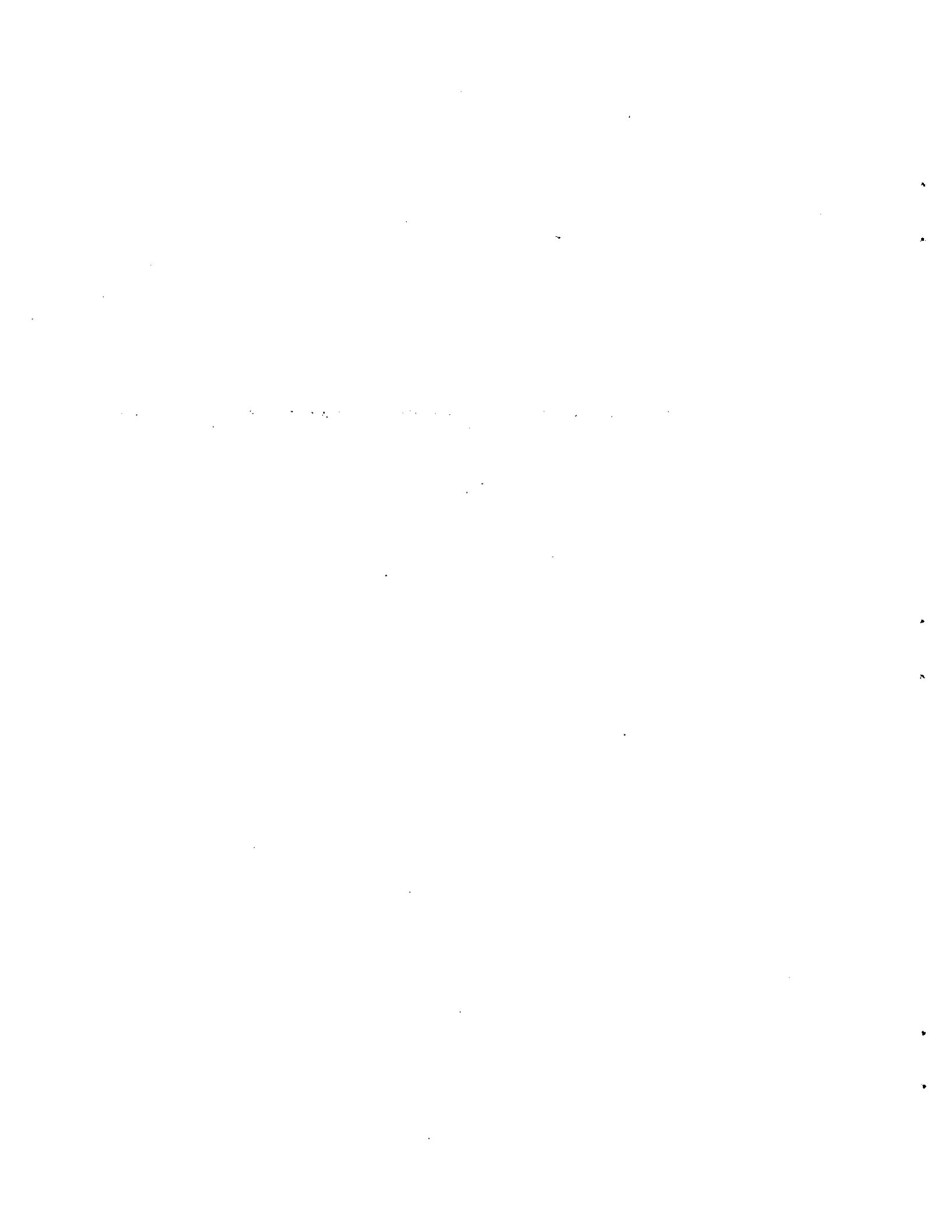


Fig. 12



Working Papers, Preprints, and Reprints in the SFI Series

- 89-001 "A Double Auction Market for Computerized Traders"
John Rust, Richard Palmer, and John H. Miller
- 89-002 "Communication, Computability and Common Interest Games"
Luca Anderlini
- 89-003 "The Coevolution of Automata in the Repeated Prisoner's Dilemma"
John H. Miller
- 89-004 "Money as a Medium of Exchange in an Economy with Artificially Intelligent Agents"
Ramon Marimon, Ellen McGrattan, and Thomas J. Sargent
- 89-005 "The Dynamical Behavior of Classifier Systems"
John H. Miller and Stephanie Forrest
- 89-006 "Nonlinearities in Economic Dynamics"
José A. Scheinkman
- 89-007 "'Silicon Valley' Locational Clusters: When Do Increasing Returns Imply Monopoly?"
W. Brian Arthur
- 89-008 "Mutual Information Functions of Natural Language Texts"
Wentian Li
- 90-001 "Learning by Genetic Algorithms in Economic Environments"
Jasmina Arifovic
- 90-002 "Optimal Detection of Nonlocal Quantum Information"
Asher Peres and William K. Wootters
- 90-003 "Artificial Life: The Coming Evolution"
J. Doyne Farmer and Alletta d'A. Belin
- 90-004 "A Rosetta Stone for Connectionism"
J. Doyne Farmer
- 90-005 "Immune Network Theory"
Alan S. Perelson
- 90-006 "Protein Evolution of Rugged Landscapes"
Catherine A. Macken and Alan S. Perelson
- 90-007 "Evolutionary Walks on Rugged Landscapes"
Catherine A. Macken, Patrick S. Hagan, and Alan S. Perelson
- 90-008 "Transition Phenomena in Cellular Automata Rule Space"
Wentian Li, Norman H. Packard, and Chris Langton
- 90-009 "Absence of $1/f$ Spectra in Dow Jones Daily Price"
Wentian Li
- 90-010 "Economic Life on a Lattice: Some Game Theoretic Results"
R. A. Cowan and J. H. Miller
- 90-011 "Algorithmic Chemistry: A Model for Functional Self-Organization"
Walter Fontana
- 90-012 "Expansion-Modification Systems: A Model for Spatial $1/f$ Spectra"
Wentian Li

- 90-013 "Coevolution of the Edge of Chaos: Coupled Fitness Landscapes, Poised States, and Coevolutionary Avalanches"
Stuart A. Kauffman and Sonke Johnsen
- 90-014 "A Short Summary of Remarks at the Meeting at the Santa Fe Institute on "Paths Toward A Sustainable Human Society""
George A. Cowan
- 90-015 "On The Application of Antiferromagnetic Fermi Liquid Theory to NMR Experiments on $YBa_2Cu_3O_{6.63}$ "
H. Monien, D. Pines, and M. Takigawa
- 90-016 "On The Application of Antiferromagnetic Fermi Liquid Theory on NMR Experiments in $La_{1.85}Sr_{0.15}CuO_4$ "
H. Monien, P. Monthous, and D. Pines
- 90-017 "Size and Connectivity as Emergent Properties of a Developing Immune Network"
Rob J. De Boer and Alan S. Perelson
- 90-018 "Game Theory Without Partitions, and Applications to Speculation and Consensus"
John Geanakoplos
- 90-019 "*Drosophila* Segmentation: Supercomputer Simulation of Prepattern Hierarchy"
Axel Hunding, Stuart A. Kauffman, and Brian C. Goodwin
- 90-020 "Random Grammars: A New Class of Models for Functional Integration and Transformation in the Biological, Neural, and Social Sciences"
Stuart A. Kauffman
- 90-021 "Visions of a Sustainable World"
Murray Gell-Mann
- 90-022 "Mutation in Autocatalytic Reaction Networks"
Peter F. Stadler and Peter Schuster
- 90-023 "Novel Perturbation Expansion for the Langevin Equation"
Carl Bender, Fred Cooper, Greg Kilcup, L.M. Simmons, Jr., and Pinaki Roy
- 90-024 "Mutual Information Functions versus Correlation Functions"
Wentian Li
- 90-025 "A Relation Between Complexity and Entropy for Markov Chains and Regular Languages"
Wentian Li
- 90-026 "A Learning Algorithm that Mimics Human Learning"
W. Brian Arthur
- 90-027 "Localized Memories in Idiotypic Networks"
G rard Weisbuch, Rob J. De Boer and Alan S. Perelson
- 90-028 "Pattern Formation in One- and Two-Dimensional Shape Space Models of the Immune System"
Rob J. De Boer, Lee A. Segel and Alan S. Perelson